Journal of Engineering Mathematics **47:** 217–250, 2003.

One-dimensional modelling of a vascular network in space-time variables

S.J. SHERWIN[1,*], V. FRANKE[1], J. PEIRÓ[1] and K. PARKER[2]
[1]*Department of Aeronautics, South Kensington Campus, Imperial College London, London, SW7 2AZ, UK;*
[2]*Department of Bioengineering, South Kensington Campus, Imperial College London, London, SW7 2AZ, UK*

Received 6 December 2002; accepted in revised form 3 September 2003

Abstract. In this paper a one-dimensional model of a vascular network based on space-time variables is investigated. Although the one-dimensional system has been more widely studied using a space-frequency decomposition, the space-time formulation offers a more direct physical interpretation of the dynamics of the system. The objective of the paper is to highlight how the space-time representation of the linear and nonlinear one-dimensional system can be theoretically and numerically modelled. In deriving the governing equations from first principles, the assumptions involved in constructing the system in terms of area-mass flux (A, Q), area-velocity (A, u), pressure-velocity (p, u) and pressure-mass flux(p, Q) variables are discussed. For the nonlinear hyperbolic system expressed in terms of the (A, u) variables the extension of the single-vessel model to a network of vessels is achieved using a characteristic decomposition combined with conservation of mass and total pressure. The more widely studied linearised system is also discussed where conservation of static pressure, instead of total pressure, is enforced in the extension to a network. Consideration of the linearised system also allows for the derivation of a reflection coefficient analogous to the approach adopted in acoustics and surface waves. The derivation of the fundamental equations in conservative and characteristic variables provides the basic information for many numerical approaches. In the current work the linear and nonlinear systems have been solved using a spectral/hp element spatial discretisation with a discontinuous Galerkin formulation and a second-order Adams-Bashforth time-integration scheme. The numerical scheme is then applied to a model arterial network of the human vascular system previously studied by Wang and Parker (To appear in *J. Biomech.* (2004)). Using this numerical model the role of nonlinearity is also considered by comparison of the linearised and nonlinearised results. Similar to previous work only secondary contributions are observed from the nonlinear effects under physiological conditions in the systemic system. Finally, the effect of the reflection coefficient on reversal of the flow waveform in the parent vessel of a bifurcation is considered for a system with a low terminal resistance as observed in vessels such as the umbilical arteries.

Key words: branching flows, linearised reflection coefficient, 1D flow modelling, spectral/hp element methods, vascular network

1. Introduction

The one-dimensional modelling of the human arterial system was introduced by Euler in 1775 [1] who derived the partial differential equations expressing the conservation of mass and momentum for inviscid flow. In order to close the problem, he also suggested two possible, but experimentally unrealistic, constitutive equations describing the behaviour of the elastic wall with changes in the lumenal pressure. Apparently, he did not recognise the wave-like nature of the flow and was not able to find a solution for his equations, citing "insuperabiles difficultates". The wave nature of the arterial flow was first described scientifically by Young

*s.sherwin@imperial.ac.uk

[2] who derived the wave speed using an argument based on intuition and analogy to Newton's theory of the speed of sound in air. In 1877 Moens [3] and Korteweg [4] independently published analyses of flow in thin-walled elastic vessels, deriving what is now known as the Moens-Korteweg equation for the wave speed. Riemann [5] (1860) provided the analytical tools for the general equations when he introduced the method of characteristics, which was first applied to arterial flow more than 50 years ago, most notably by Anliker and co-workers [6, 7] and Skalak [8].

The equations derived by Euler are a system of nonlinear partial differential equations analogous to the shallow-water equations of hydrodynamics or the one-dimensional inviscid equations of gas dynamics. However, under physiological conditions of the human arterial system, the equations are only weakly nonlinear and therefore many characteristics of the flow can be captured by the linearised system. This is essentially the approach of Womersley [9] (1957) who linearised the two-dimensional equations for flow in straight, circular elastic tubes and obtained the wave solution by Fourier techniques. This linear analysis has become the 'standard' model of waves in the arteries found in most haemodynamics textbooks. The success of the linearised model and the apparently periodic nature of the arterial system has led most investigators since Womersley to analyse arterial flow in the frequency rather than the time domain using the so-called "electrical" analogy.

Although there is a large body of work using the frequency domain analysis, many facets of the physiological waveforms have yet to be explained. It is the conjecture of the authors that consideration of the solution in the frequency domain is potentially limiting. The reasons for this are twofold. Firstly the frequency domain can lead to the implicit assumption that the arterial system is in a state of "steady oscillation" implying that the system will remain oscillating even when the forcing from the heart is stopped. However, the characteristic speed of wave propagation is sufficiently fast that the time scale to propagate information through the whole arterial system is much smaller than the duration of the cardiac cycle. It is generally observed in resting conditions that flow in the large arteries comes to rest during late diastole. More convincingly, during ectopic beats when contraction of the heart is blocked or is so ineffectual that the aortic valve never opens, neither the flow nor the pressure shows any hint of the previous "periodic" behaviour. Secondly, the aortic valve is an essentially nonlinear element dividing the cardiac cycle into systole when the ventricle is open to the arteries and diastole when it is closed. Since the frequency domain analyses cannot distinguish between systole and diastole, identical systolic behaviour of the ventricle would result in different input power spectra at different heart rates. Since the fraction of the cardiac cycle occupied by systole varies significantly with heart rate, much of the characteristic behaviour of the ventricle during systole (and the arterial system during diastole) could be masked simply by changes in the fundamental frequency.

An alternative approach to analyse the one-dimensional arterial system is to use the method of characteristics in the time-space domain. The rest of the paper is strongly motivated by the work of Wang and Parker [10, 11] who used a semi-analytical time-space domain approach to model the linearised wave motion in arteries. In their model they used a highly idealised cardiac function in a fairly realistic model of the anatomy of the largest arteries and based their arterial model on the data of Westerhof and Noordergraaf [12]. The method of characteristics has also previously been applied to the study of waves by Skalak [8], Stettler *et al.* [6, 7] and Stergiopulos *et al.* [13].

The objective of this paper is to review the one-dimensional model starting from first principles and to demonstrate how these equations can be applied to linear and nonlinear numerical

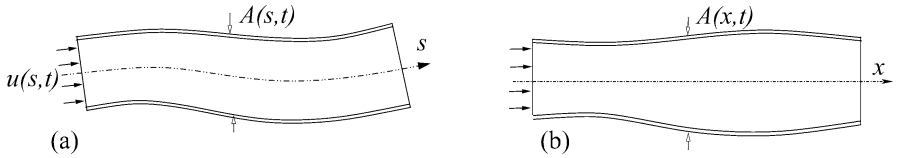

Figure 1. Nomenclature for the model of a one-dimensional vessel. (a) General orientation, (b) One-dimensional orientation.

modelling of a vascular network. Furthermore, we derive classical linear results, such as the reflection coefficient, which are insightful in analysing the system since the nonlinearities under many physiological conditions are relatively weak.

The paper is organised as follows, in Section 2 we detail the derivation of the governing equations by considering the conservation of mass and momentum for a single one-dimensional vessel. Introducing the concept of a sectional algebraic pressure-area relationship we then outline different combinations of the governing equations in terms of the variables pressure p, area A, velocity u and flowrate Q. Using the (A, u) system we subsequently construct both the linear and nonlinear systems in terms of characteristic variables.

In Section 2.2 we extend the single-vessel formulation to a network by considering the modelling of junctions including both bifurcations, and the topologically similar, merging flow junctions. Having introduced the junction modelling we can then derive the linearised reflection and transmission coefficients [15, Chapter 2] which are the direct analogy to the coefficients commonly applied in acoustics and surface waves [14, Chapter 8]. Finally, to complete the network description, boundary conditions at the outflow are required which are enforced using a terminal resistance which forces the incoming wave to be the scaled reflection of the outgoing wave [11, 13].

In Section 3 we outline the numerical discretisation of the governing (A, u) system using a discontinuous Galerkin formulation with a one-dimensional spectral/hp element spatial approximation. This formulation allows us to combine the fast convergence and good dispersion properties, commonly associated with the spectral methods, with the geometric flexibility to discretise each vessel in the branching network. Finally, in Section 4 we apply the one-dimensional model to a branching network containing 55 arteries, previously studied by Wang and Parker [10, 11], as well as analysing the effect of bifurcation reflections on flow waveforms in a model system with low terminal resistance.

2. Problem formulation

2.1. Governing equations for a single vessel

Consider a vessel of length l with a centreline described by $s(\mathbf{x})$ and cross sectional area normal to s denoted by $A(s, t)$ as indicated in Figure 1(a). Our first modelling simplification will be to assume that the local curvature is everywhere small enough so that the axial direction can be described by a Cartesian coordinate x as shown in Figure 1(b) so that the problem can be defined in one-dimension. At each cross section we define $A(x, t) = \int_S \mathrm{d}\sigma$ as the area of the cross section S and $u(x, t) = \frac{1}{A}\int_S \hat{u}\mathrm{d}\sigma$, $p(x, t) = \frac{1}{A}\int_S \hat{p}\mathrm{d}\sigma$ as the average velocity and internal pressure over the cross section where $\hat{u}(x, \sigma, t)$ and $\hat{p}(x, \sigma, t)$ denote the values of velocity and pressure within a constant x-section. We also introduce the dependent variable $Q(x, t) = Au$ which represents the volume flux at a given section.

We therefore have three independent variables A, u, p or equivalently A, Q, p. The required three independent equations will be provided by the equations of conservation of mass and momentum and a constitutive equation relating cross sectional area to internal pressure. In what follows, we shall also assume that the fluid is incompressible and Newtonian and so the density ρ and dynamic viscosity μ are constant. Our final modelling assumption is that the structural arterial properties are constant at a section.

In the Sections 2.1.1 and 2.1.2 we shall derive conservation of the mass and momentum equations starting from a control volume statement. As we shall see in Section 2.1.1, applying the mass conservation statement to a control volume allows us to derive the Windkessel equation commonly used in reduced modelling of the arterial system [16]. This statement does not, however, inform us about the dynamics of the system along the vessel which is where the one-dimensional system proves to be more insightful. The dynamics of the one-dimensional system are more easily understood in terms of the characteristic variables which are derived in Section 2.1.5. However, before doing so, we define the pressure area relationship and alternative forms of the mass and momentum equations in Sections 2.1.3 and 2.1.4.

2.1.1. *Mass-conservation equation*

Defining the vessel shown in Figure 1(b) as our control volume, conservation of mass requires that the rate of change of mass within the control volume plus the net mass flux out of the control volume is zero. Denoting the volume as $V(t) = \int_0^l A \, \mathrm{d}x$, where l is the length of the vessel and assuming there is no seepage through the side walls, we can write the mass conservation as

$$\rho \frac{\mathrm{d}V(t)}{\mathrm{d}t} + \rho Q(l,t) - \rho Q(0,t) = 0. \tag{1}$$

If seepage does occur, a source term can be included to accommodate this contribution.

To determine the one-dimensional equation of mass conservation, we insert $V(t) = \int_0^l A(x,t)\mathrm{d}x$ in Equation (1) and note that

$$Q(l,t) - Q(0,t) = \int_0^l \frac{\partial Q}{\partial x}\mathrm{d}x$$

to obtain

$$\rho \frac{\mathrm{d}}{\mathrm{d}t} \int_0^l A(x,t)\mathrm{d}x + \rho \int_0^l \frac{\partial Q}{\partial x}\mathrm{d}x = 0.$$

If we assume l is independent of time, we can take the time derivative inside the integral to arrive at

$$\rho \int_0^l \left\{ \frac{\partial A}{\partial t} + \frac{\partial Q}{\partial x} \right\} \mathrm{d}x = 0.$$

Since we have not specified the length l, the control volume is arbitrary and so the above equation must be true for any value of l and so in general we require that the integrand is zero. We therefore obtain the differential one-dimensional mass conservation equation

$$\frac{\partial A}{\partial t} + \frac{\partial Q}{\partial x} = \frac{\partial A}{\partial t} + \frac{\partial uA}{\partial x} = 0. \tag{2}$$

Remark: The control volume statement (1) can be used to obtain the time variation of the "Windkessel" pressure as originally discussed by Frank [17]. Introducing the vessel compliance C, defined as $C = \frac{\mathrm{d}V}{\mathrm{d}P}$ where P is an appropriate average of the pressure p over length l, and applying the chain rule in conjunctions with Equation (1) leads to

$$\frac{\mathrm{d}P}{\mathrm{d}t} = \frac{\mathrm{d}P}{\mathrm{d}V}\frac{\mathrm{d}V}{\mathrm{d}t} = \frac{Q(0,t) - Q(l,t)}{C}. \tag{3}$$

The definition of compliance as a constant implicitly assumes a uniform variation of pressure within the volume of the vessel. Therefore if we know the inflow flux $Q(0,t)$ and define a relationship between $Q(l,t)$ and pressure $P(t)$, then Equation (3) can be integrated to determine a temporal pressure variation within the vessel. Normally the outflow is assumed to be related to the pressure by a momentum-type relationship of the form $Q(l,t) = (P(t) - P_\infty)/R$, where P_∞ is an asymptotic pressure and R is the effective resistance of the peripheral systemic circulation. Nevertheless, we recall that it is the pressure gradient which drives the flow within the vessel and so the uniform in space temporal pressure variation does not significantly affect the dynamics of the flow velocity. As noted in recent work by Wang *et al.* [18], the temporal Windkessel pressure does, however, contribute to the late-diastole pressure-time history within the vessels.

2.1.2. *Momentum equation*

Again we consider the vessel as our control volume and assume that there is no flux through the side walls in the x-direction. The momentum equation states that the rate of change of momentum within the control volume plus the net flux of momentum out of the control volume is equation to the applied forces on the control volume and can be stated over an arbitrary length l as

$$\frac{\mathrm{d}}{\mathrm{d}t}\int_0^l \rho Q \mathrm{d}x + (\alpha\rho Q u)_l - (\alpha\rho Q u)_0 = F, \tag{4}$$

where we recall that $Q = Au$ and define F as the applied forces in the x-direction acting on the control volume. Since $\rho Q = \rho u A = \rho \int_S \hat{u}\mathrm{d}\sigma$ represents the x-momentum integrated over the section S, the left-hand side of Equation (4) is analogous to the left-hand side of the mass conservation given by Equation (1). However, in the momentum balance we have introduced a momentum flux correction factor 'α' which accounts for the nonlinearity of the sectional integration in terms of the local velocity $\hat{u}$, *i.e.*,

$$\int_S \rho(\hat{u})^2 \mathrm{d}\sigma \equiv \alpha\rho u^2 A = \alpha\rho Q u \qquad \Rightarrow \qquad \alpha(x,t) = \frac{\int_S \hat{u}^2 \mathrm{d}\sigma}{Au^2}.$$

When the the flow profile is uniform over a section, $\alpha = 1$.

To complete Equation (4) we need to define the applied forces F which typically involve a pressure and viscous force contribution, *i.e.*,

$$F = (pA)_0 - (pA)_l + \int_0^l \int_{\partial S} \hat{p} n_x \mathrm{d}s \mathrm{d}x + \int_0^l f \mathrm{d}x, \tag{5}$$

where ∂S is the boundary of section S, n_x is the x-component of the surface normal and f represents is the friction force per unit length. The side wall pressure force given by the

double integral can be simplified by assuming constant sectional pressure and treating the tube as axisymmetric, the term becomes

$$\int_0^l \int_{\partial S} \hat{p} n_x \mathrm{d}s \mathrm{d}x = \int_0^l p \frac{\partial A}{\partial x} \, \mathrm{d}x. \tag{6}$$

Finally, if we combine Equations (4), (5) and (6), we obtain the control-volume statement of momentum conservation

$$\frac{\mathrm{d}}{\mathrm{d}t} \int_0^l \rho Q \mathrm{d}x + (\alpha \rho Q u)_l - (\alpha \rho Q u)_0 = (pA)_0 - (pA)_l + \int_0^l p \frac{\partial A}{\partial x} \, \mathrm{d}x + \int_0^l f \mathrm{d}x. \tag{7}$$

To obtain the one-dimensional differential momentum equation we observe that

$$(\alpha \rho Q u)_l - (\alpha \rho Q u)_0 = \int_0^l \frac{\partial (\alpha \rho Q u)}{\partial x} \, \mathrm{d}x, \quad (pA)_0 - (pA)_l = -\int_0^l \frac{\partial (pA)}{\partial x} \, \mathrm{d}x$$

which, upon insertion in (7) and assuming l is independent of time and ρ is constant, gives us

$$\rho \int_0^l \left\{ \rho \frac{\partial Q}{\partial t} + \rho \frac{\partial (\alpha Q u)}{\partial x} \right\} \, \mathrm{d}x = \int_0^l \left\{ -\frac{\partial (pA)}{\partial x} + p \frac{\partial A}{\partial x} + f \right\} \, \mathrm{d}x.$$

Once again this relationship is satisfied for an arbitrary length l and so can only be satisfied when the integrands are equal. The one-dimensional momentum equation becomes

$$\frac{\partial Q}{\partial t} + \frac{\partial (\alpha Q u)}{\partial x} = -\frac{A}{\rho} \frac{\partial p}{\partial x} + \frac{f}{\rho}, \tag{8}$$

where we have simplified the right-hand side pressure gradient terms.

2.1.3. *Pressure-area relationship and distensibility*

The mass and momentum Equations (2) and (8) give us two equations with three unknowns A, u and p or alternatively A, Q and p. We need to close the system by defining an explicit algebraic relationship between the sectional pressure p and area A. In the following analysis we restrict our attention to sectional algebraic relationships functionally denoted by

$$p = \mathcal{F}(A; x, t). \tag{9}$$

The pressure is assumed to be dependent upon the area and its derivatives. The area is therefore implicitly dependent upon time and space. Although the wall properties of a vessel alter the scaling of the relationship (9), they are not independent variables although they may depend upon the area.

From the functional form of the pressure area relationship we define the distensibility D as:

$$D = \frac{1}{A} \frac{\mathrm{d}A}{\mathrm{d}p}. \tag{10}$$

The algebraic form we will adopt later in this paper assumes a thin wall tube where each section is independent of the others. Using Laplace's law leads to a pressure area relationship of the form

$$p = p_{\text{ext}} + \beta(\sqrt{A} - \sqrt{A_0}), \tag{11}$$

where

$$\beta(x) = \frac{\sqrt{\pi}h_0 E}{(1-\nu^2)A_0}.$$

Here $h_0(x)$ and $A_0(x)$ denote the vessel-wall thickness and sectional area at the equilibrium state $(p, u) = (p_{\text{ext}}, 0)$, $E(x)$ is the Young's modulus, p_{ext} is the constant external pressure, and ν is the Poisson ratio, typically taken to be $\nu = 1/2$ since biological tissue is practically incompressible. The distensibility for the pressure relation (11) is

$$D = \frac{2}{\beta\sqrt{A}}.$$

2.1.4. *The* (A, u), (A, Q), (p, u) *and* (p, Q) *systems*

We can write the governing one-dimensional system in terms of the variables (A, Q) as

$$\frac{\partial A}{\partial t} + \frac{\partial Q}{\partial x} = 0, \tag{12}$$

$$\frac{\partial Q}{\partial t} + \frac{\partial \alpha Q^2/A}{\partial x} = -\frac{A}{\rho}\frac{\partial p}{\partial x} + \frac{f}{\rho}. \tag{13}$$

This system, together with the pressure-area relation, is one of the most general form of one-dimensional models and has been used in [19]. This system, with a slightly different pressure relationship, has been shown by Canic and Kim [20] to lead to smooth solutions under some reasonable conditions on the smoothness of boundary and initial data. Two critical assumptions needed to reach this conclusion are the pulsatility of the inflow data and a bound on the length of the tube, both are verified for physiological flows in the human arterial tree. In the same work it is also shown that, if the solution is smooth and the initial and boundary data are such that $A > 0$, A remains strictly positive for all times. Finally we note that Formaggia *et al.* [19] also used system (12–13) to derive an energy inequality which bounds a measure of the energy of the hyperbolic system, as well as an an entropy function for the system.

Alternatively we can write the system in terms of the variables (A, u). To manipulate the momentum Equation (13) it is convenient to write it as

$$u\left\{\frac{\partial A}{\partial t} + \frac{\partial uA}{\partial x}\right\} + u\frac{\partial(\alpha-1)uA}{\partial x} + A\left\{\frac{\partial u}{\partial t} + \alpha u\frac{\partial u}{\partial x}\right\} = -\frac{A}{\rho}\frac{\partial p}{\partial x} + \frac{f}{\rho},$$

where the first bracketed expression is the mass conservation equation (12) and is therefore zero.

If we assume inviscid flow with a flat velocity profile, which implies that $\alpha = 1$ and $f = 0$, we can write the one-dimensional system in terms of the (A, u) variables as

$$\frac{\partial A}{\partial t} + \frac{\partial uA}{\partial x} = 0, \tag{14}$$

$$\frac{\partial u}{\partial t} + \frac{\partial u^2/2}{\partial x} = -\frac{1}{\rho}\frac{\partial p}{\partial x}. \tag{15}$$

In both the systems (12–13) and (14–15) we can introduce the pressure area relationship through the pressure gradient term by noting that

$$\frac{\partial p}{\partial x} = \frac{1}{DA}\frac{\partial A}{\partial x} + r(x). \tag{16}$$

Here we observe that $A = A(p)$ and $r(x)$ represents the other spatial dependencies in the pressure area relationship. For example, in the pressure-area relationship given by Equation (11)

$$r = \frac{\partial p}{\partial \beta}\frac{\partial \beta}{\partial x} + \frac{\partial p}{\partial A_0}\frac{\partial A_0}{\partial x}.$$

Finally, from a clinical perspective, it is convenient to consider the system in terms of the variables (p, u) or (p, Q), since these are the physically measurable variables in a clinical environment. Using the definition of distensibility and assuming β and A_0 are constant, we obtain

$$\frac{\partial A}{\partial t} = DA\frac{\partial p}{\partial t} \quad \text{and} \quad \frac{\partial A}{\partial x} = DA\frac{\partial p}{\partial x}.$$

The inviscid one-dimensional system can now be written in terms of the (p, u) variables as

$$\frac{\partial p}{\partial t} + u\frac{\partial p}{\partial x} + \frac{1}{D}\frac{\partial u}{\partial x} = 0, \tag{17}$$

$$\frac{\partial u}{\partial t} + \frac{\partial u^2/2}{\partial x} = -\frac{1}{\rho}\frac{\partial p}{\partial x}. \tag{18}$$

Alternatively we can combine Equations (17) and (13) to define the governing one-dimensional system in terms of the variables (p, Q) as

$$\frac{\partial p}{\partial t} + u\frac{\partial p}{\partial x} + \frac{1}{D}\frac{\partial u}{\partial x} = 0, \tag{19}$$

$$\frac{\partial Q}{\partial t} + \frac{\partial \alpha Q^2/A}{\partial x} = -\frac{A}{\rho}\frac{\partial p}{\partial x} + \frac{f}{\rho}. \tag{20}$$

We also note that in the above system we have not assumed an inviscid flat profile and so have left α and f in the second equation.

In summary, we note that the most general system derived in this section is represented in terms of the (A, Q) variables as given by Equations (12) and (13). Under the assumption of inviscid flow with a flat velocity profile we can obtain a form in terms of the variables (A, u) as given by Equations (14) and (15) both systems also require an algebraic pressure area relationship. We also note that the (A, u) system has a very compact conservative form which will lead us to adopt this form in the next section. The most restrictive system is the system described by Equations (17–18) in terms of the (p, u) variables. Here we have assumed inviscid flow with a flat velocity profile and that material properties, β and equilibrium area A_0 are constant. Finally the (p, Q) system, given by Equations (19–20), requires the assumption of constant material properties and equilibrium area but does not assume an inviscid, flat velocity profile.

2.1.5. *The characteristic system*

Considering Equations (14) and (15) with the pressure-area relationship (11), when β and A_0 are constant, we can write the system in non-conservative form as

$$\frac{\partial \boldsymbol{U}}{\partial t} + \boldsymbol{H}(\boldsymbol{U})\frac{\partial \boldsymbol{U}}{\partial x} = \boldsymbol{0}, \tag{21}$$

where

$$\boldsymbol{U} = \begin{bmatrix} A \\ u \end{bmatrix} \qquad \boldsymbol{H} = \begin{bmatrix} u & A \\ \frac{1}{\rho D A} & u \end{bmatrix},$$

and we have also applied Equation (16).

Under the assumption that $A > 0$,indeed a necessary condition to have a physically relevant solution, the matrix $\boldsymbol{H}$ has two real eigenvalues

$$\lambda_{1,2}(\boldsymbol{H}) = u \pm c,$$

where $c = \frac{1}{\sqrt{\rho D}}$ is the wave speed for the nonlinear system. For typical values of velocity, vessel area and the elastic parameter β encountered in arteries under physiological conditions, we find that $\lambda_1 > 0$ and $\lambda_2 < 0$.

In system (21) the matrix of left eigenvalues, $\boldsymbol{L}$, of $\boldsymbol{H}$ can be written as

$$\boldsymbol{L} = \begin{bmatrix} \frac{c}{A} & 1 \\ -\frac{c}{A} & 1 \end{bmatrix}, \tag{22}$$

where

$$\boldsymbol{L}\boldsymbol{H} = \boldsymbol{\Lambda}\boldsymbol{L} \qquad \text{and} \qquad \boldsymbol{\Lambda} = \begin{bmatrix} \lambda_1 & 0 \\ 0 & \lambda_2 \end{bmatrix}.$$

Noting that $\boldsymbol{H} = \boldsymbol{L}^{-1}\boldsymbol{\Lambda}\boldsymbol{L}$ and premultiplying system (21) by $\boldsymbol{L}$, we obtain

$$\boldsymbol{L}\frac{\partial \boldsymbol{U}}{\partial t} + \boldsymbol{\Lambda}\boldsymbol{L}\frac{\partial \boldsymbol{U}}{\partial x} = \boldsymbol{0}. \tag{23}$$

Finally we can introduce a change of variables such that $\frac{\partial \boldsymbol{W}}{\partial \boldsymbol{U}} = \boldsymbol{L}$ where $\boldsymbol{W} = [W_1, W_2]^T$ is the vector of characteristic variables which transforms Equation (23) into

$$\frac{\partial \boldsymbol{W}}{\partial t} + \boldsymbol{\Lambda}\frac{\partial \boldsymbol{W}}{\partial x} = \boldsymbol{0},$$

which is a system of decoupled scalar equations, *i.e.*,

$$\frac{\partial W_1}{\partial t} + \lambda_1 \frac{\partial W_1}{\partial x} = 0, \tag{24}$$

$$\frac{\partial W_2}{\partial t} + \lambda_2 \frac{\partial W_2}{\partial x} = 0. \tag{25}$$

The scaling of $\boldsymbol{L}$ in (22) was chosen so that $\frac{\partial^2 W_{1,2}}{\partial A \partial u} = \frac{\partial^2 W_{1,2}}{\partial u \partial A}$ and we can determine the characteristic variables as

$$W_{1,2} = \int_{u_0}^{u} \mathrm{d}u \pm \int_{A_0}^{A} \frac{c}{A}\,\mathrm{d}A = u - u_0 \pm \int_{A_0}^{A} \frac{c}{A}\,\mathrm{d}A, \tag{26}$$

where (u_0, A_0) is taken as a reference state. The characteristic variables given by Equation (26) are also the Riemann invariants of the system (14) and (15) in terms of the (A, u) variables.

For the pressure area relationship defined in Equation (11) we can derive an explicit form of $\boldsymbol{W}$. Recalling that $c = 1/\sqrt{\rho D}$ and evaluating D for the pressure area relationship (11), we obtain

$$W_{1,2} = u \pm 4(c - c_0) = u \pm 4\sqrt{\frac{\beta}{2\rho}}\left(A^{1/4} - A_0^{1/4}\right), \tag{27}$$

where we have assumed that $u_0 = 0$ when $A = A_0$. The above result is also obtained by Formaggia *et al.* [19, 21] who considered the more general (A, Q) system.

System (21) can be linearised about the diastolic conditions $A = A_0$ and $u = 0$. Denoting the linearised perturbation variables for area and velocity as a and u', respectively, inserting $u = u'$ and $A = A_0 + a$ into Equation (21) and ignoring quadratic terms, we obtain

$$\frac{\partial \boldsymbol{U}_0}{\partial t} + \boldsymbol{H}_0 \frac{\partial \boldsymbol{U}_0}{\partial x} = 0, \tag{28}$$

where

$$\boldsymbol{U}_0 = \begin{bmatrix} a \\ u' \end{bmatrix}, \qquad \boldsymbol{H}_0 = \begin{bmatrix} 0 & A_0 \\ \frac{1}{\rho D_0 A_0} & 0 \end{bmatrix} \quad \text{and} \quad D_0 = D(A_0).$$

Following a similar derivation as for the nonlinear system the linearised wave speed is $\lambda^0_{1,2}(\boldsymbol{H}_0) = \pm c_0$ where $c_0 = \frac{1}{\sqrt{\rho D_0}}$ and the linearised characteristic variables $\boldsymbol{W}^0 = [W^0_1, W^0_2]^T$ are

$$W^0_{1,2} = u' \pm \int_{A_0}^{A} \frac{c_0}{A_0}\, \mathrm{d}A = u' \pm \frac{c_0}{A_0} a. \tag{29}$$

Finally we also observe that the expression of the characteristic variables in terms of (p, u) can also be obtained from first principles or by using the distensibility definition in Equation (26) since,

$$W_{1,2}(p, u) = \int_{u_0}^{u'} \mathrm{d}u \pm \int_{p_0}^{p} \frac{c}{A} \frac{\mathrm{d}A}{\mathrm{d}P}\, \mathrm{d}P = u' \pm \int_{p_0}^{p} cD\, \mathrm{d}P. \tag{30}$$

For the linearised (p, u) system, Equation (30) can be integrated to determine

$$W^0_{1,2}(p, u) = u' \pm \int_{p_0}^{p} c_0 D_0\, \mathrm{d}P = u' \pm \frac{p'}{\rho c_0} \tag{31}$$

where $D_0 = 1/(\rho c_0^2)$ and $p = p_0 + p'$.

2.2. JUNCTIONS, THE LINEAR REFLECTION COEFFICIENT AND TERMINAL RESISTANCE

2.2.1. *Splitting flows at junctions*

The one-dimensional model of the compliant tube can be extended to handle the arterial tree by imposing suitable interface conditions at the bifurcations or branching points of the tree. Assuming we have an initial compatible state (A^i, u^i) within each vessel of the bifurcation, we need to determine the values of the variables (A, u) in all vessels at a later time. The variables (A, u), as well as A_0 and β can all be discontinuous at a junction and so the solution at this point can be considered as the solution to a Riemann problem.

From the decomposition (24–25) into characteristic variables W_1, W_2 of the governing system (14–15) we know that the system can be interpreted in terms of a forward- and a backward-travelling waves.

Consider the model bifurcation configuration shown in Figure 2 where we denote the parent vessel by an index 1 and the upper and lower daughter vessels by the indices 2 and 3, respectively. At the bifurcation we have six unknowns: (A_1, u_1) in the parent vessel; (A_2, u_2) in the upper daughter vessel and (A_3, u_3) in the lower daughter vessel.

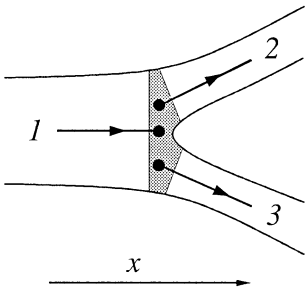

Figure 2. Notation for arterial tree bifurcation.

Looking at the problem from a characteristics point of view, information can only reach the bifurcation from within vessel 1 by a forward-travelling wave. The forward-travelling wave is governed by Equation (24) in terms of the characteristic variable W_1^1 that according to Equation (27) is a function of (A_1, u_1). Here the superscript denotes the vessel number. Similarly, within the daughter vessels information can only reach the bifurcation by a backwards-travelling wave which is governed by Equation (25) with characteristic variables $W_2^2(A_2, u_2)$ or $W_2^3(A_3, u_3)$. The hyperbolic nature of the problem reduces the incoming information to three constant characteristic variables W_1^1, W_2^2 and W_2^3. The first three equations of the Riemann problem are obtained by imposing that the characteristic variables in each vessel should remain constant. From the definition of the characteristic variables for the nonlinear system, given by Equation (27), we have

$$u_1 + 4(c_1 - c_0^1) = W_1^1, \tag{32}$$

$$u_2 - 4(c_2 - c_0^2) = W_2^2, \tag{33}$$

$$u_3 - 4(c_3 - c_0^3) = W_2^3, \tag{34}$$

where c_0^1, c_0^2, c_0^3 are the values of the wave speed c evaluated using the equilibrium area A_0 in vessels 1, 2 and 3, respectively.

To close the problem we require another three independent equations. The first condition is physically motivated by requiring that the mass is conserved through the bifurcation and therefore mass flux balance results in $Q_1 = Q_2 + Q_3$. The other two conditions are obtained from the requirement of continuity of the momentum flux at the bifurcation. This leads to the condition that total pressure $p + \frac{1}{2}\rho u^2$ should be continuous at the boundary. These requirements provide the three additional equations:

$$A_1 u_1 = A_2 u_2 + A_3 u_3, \tag{35}$$

$$p_1 + \frac{1}{2}\rho u_1^2 = p_2 + \frac{1}{2}\rho u_2^2, \tag{36}$$

$$p_1 + \frac{1}{2}\rho u_1^2 = p_3 + \frac{1}{2}\rho u_3^2. \tag{37}$$

For the linearised system (28) the continuity of flux in the momentum equation leads to the equivalent condition that the static pressure should be continuous through the bifurcation.

In summary, the six equations given by (32–37) define a nonlinear system of algebraic equations which determine the values (A_1, u_1), (A_2, u_2) and (A_3, u_3) at the bifurcation. The inputs to the system are the material properties of the vessels β or equivalently D, the vessel

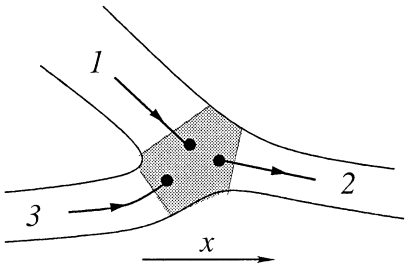

Figure 3. Notation for merging flow junction.

equilibrium areas A_0 at the bifurcation and the values of W_1^1, W_2^2 and W_2^3 which can be evaluated from the initial equilibrium state (A^i, u^i) in each vessel. The solution to this Riemann problem is used to evaluate an upwind flux at the junction in the numerical discretisation as discussed in Section 3.

2.2.2. *Merging flows at junctions*

Although considerable attention has been paid to the analysis of splitting of flows at arterial junctions, it is also of interest to study flows that merge at junctions. This is a common situation in veins and at a number of junctions in the systemic arteries, such as the junction between the vertebral arteries and the basilar artery at the base of the brain. It is also important in surgical interventions such as arterial bypass grafting where an anastomosis or cross-connection is surgically introduced to provide an alternative path around a blockage typically caused by atheromatous disease.

The conditions at the junction can be derived as previously. The downstream daughter vessels (labelled 2 and 3) in Figure 3 are orientated in opposite directions to the splitting-flow case of Section 2.2.1. Forward-travelling characteristic waves bring information to the junction in both vessels 1 and 3. The only backward-travelling information arrives at the junction from vessel 2. The merging junction therefore uses the following characteristic equations

$$u_1 + 4(c_1 - c_0^1) = W_1^1, \tag{38}$$

$$u_2 - 4(c_2 - c_0^2) = W_2^2, \tag{39}$$

$$u_3 + 4(c_3 - c_0^3) = W_1^3. \tag{40}$$

Mass conservation now becomes

$$A_1 u_1 + A_3 u_3 = A_2 u_2. \tag{41}$$

Since continuity of total pressure remains unchanged the six equations given by (36–41), define a nonlinear system of algebraic equations which determine the values (A_1, u_1), (A_2, u_2) and (A_3, u_3) at the anastomosis.

We observe that the merging flow of Figure 2 and the splitting flow shown in Figure 3 are geometrically similar. A transformation $x \to -x$ and swapping the numbering of vessel 1 and 2 in Figures 2 and 3 or, alternatively, a transformation $u_3 \to -u_3$ will map one flow into the other since under this mapping $W_2^3 = -W_1^3$.

2.2.3. *Linear reflection coefficient, R_f*

Under physiological conditions it is argued that the nonlinearity of the (A, u) system (14),(15) is relatively small. Therefore, it is of interest to study the role of junctions such as splitting and

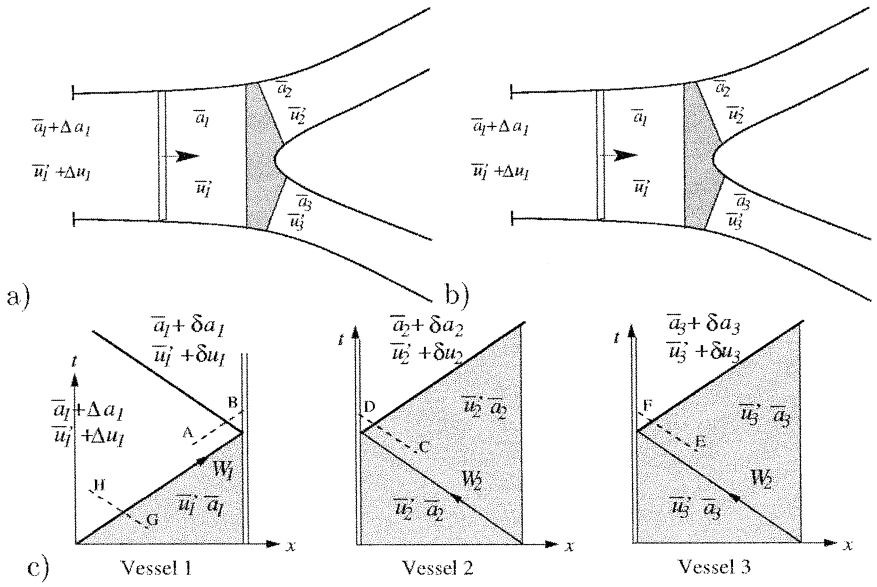

Figure 4. Linearised wave reflecting off a bifurcation. a) Configuration just before the perturbation meets the bifurcation. b) Configuration just after the perturbation meets the bifurcation. c) Characteristic *x,t* plot of each vessel during reflection.

merging flow at junctions under the assumptions of the linearised system. Classical analysis in related linearised problems of acoustics and surface waves [14, Chapter 8], [15, Chapter 2] has adopted the use of a reflection coefficient when a wave meets a boundary. As originally demonstrated by Frank [17], it is also possible to obtain a reflection coefficient, R_f, for the linearised system relating the jump in velocity, area or pressure of an incoming perturbation to the reflected jump in velocity, area or pressure.

To derive the reflection coefficient, R_f, we consider the configuration shown in Figure 4(a) where a perturbation of Δu_1, Δa_1 on the equilibrium conditions (denoted by overbars) leads to a forward-travelling wave in vessel 1. After reaching the junction there is a change in the equilibrium state so that there is a perturbation travelling in all vessels denoted by δu, δa.

As with the nonlinear system we start by considering the characteristic information approaching the junction which for the linear system can be simplified into a perturbation form. We note that the forward travelling linearised characteristic W_1^0 in vessel 1, just after the wave reaches the junction, must be constant. Considering a characteristic line such as *A*-*B* in Figure 4(a) we know that along this characteristic

$$\bar{u}_1' + \delta u_1 + \frac{c_0^1}{A_0^1}(\bar{a}_1 + \delta a_1) = W_1^0 \tag{42}$$

and, just before the reflection, we also know that

$$W_1^0 = \bar{u}_1' + \Delta u_1 + \frac{c_0^1}{A_0^1}(\bar{a}_1 + \Delta a_1). \tag{43}$$

Combining Equations (42) and (43) allows us to eliminate W_1^0. The linearity of the characteristic equations also implies that

$$\delta u_1 + \frac{c_0^1}{A_0^1}\delta a_1 = \Delta u_1 + \frac{c_0^1}{A_0^1}\Delta a_1. \tag{44}$$

A similar process for the backwards-travelling linear waves, W_2^0 in vessels 2 and 3 (see lines *C-D* and *E-F* in Figure 4(c)) leads to the analogous conditions

$$\delta u_2 - \frac{c_0^2}{A_0^2}\delta a_2 = 0, \tag{45}$$

$$\delta u_3 - \frac{c_0^3}{A_0^3}\delta a_3 = 0. \tag{46}$$

We require three additional equations to solve the six perturbation states. This is once again provided by linearised mass-flux conservation, and in the case of the linear equations, pressure continuity. Mass conservation for the linearised system reads as

$$A_0^1\delta u_1 = A_0^2\delta u_2 + A_0^3\delta u_3, \tag{47}$$

where we assume that the mass flux is conserved for the equilibrium state, *i.e.*, $A_0^1\bar{u}_1' = A_0^2\bar{u}_2' + A_0^3\bar{u}_3'$. Pressure continuity at the bifurcation implies that $\delta p_1 = \delta p_2 = \delta p_3$ which provides the two final equations in terms of static pressure perturbation. To close the system, we recall that the definition of distensibility for the linear system is $D_0 = D(A_0) = \frac{1}{A_0}\frac{\mathrm{d}A}{\mathrm{d}P}\Big|_{A_0}$ which upon integration about the linearised state results in

$$\delta p = \frac{1}{D_0 A_0}\delta a. \tag{48}$$

Finally, using the fact that $D_0 = 1/(\rho c_0^2)$, we can express pressure continuity in terms of area perturbations as

$$\frac{(c_0^1)^2}{A_0^1}\delta a_1 = \frac{(c_0^2)^2}{A_0^2}\delta a_2 = \frac{(c_0^3)^2}{A_0^3}\delta a_3. \tag{49}$$

Equations (44–47) and (49) represent a linear system of six equations in terms of $(\delta u, \delta a)$ within each vessel, assuming $(\Delta u_1, \Delta a_1)$ is known. Inserting Equation (44),(45) and (46) into (47) and using equation (49) to express δa_2, δa_3 in terms of δa_1, we obtain

$$\left(\frac{A_0^1}{c_0^1} + \frac{A_0^2}{c_0^2} + \frac{A_0^3}{c_0^3}\right)\delta a_1 = \left(\frac{A_0^1}{c_0^1}\right)^2 \Delta u_1 + \left(\frac{A_0^1}{c_0^1}\right)\Delta a_1. \tag{50}$$

This equation can be put into a more compact form by noticing that the changes across the forward-travelling incoming wave in vessel 1, Δu_1 and Δa_1, are related through the characteristic of any backward travelling wave, for example line *G-H* in Figure 4(c). This leads us to the condition

$$\bar{u}_1' + \Delta u_1 - \frac{c_0^1}{A_0^1}(\bar{a}_1 + \Delta a_1) = \bar{u}_1' - \frac{c_0^1}{A_0^1}\bar{a}_1$$

which simplifies to

$$\Delta u_1 - \frac{c_0^1}{A_0^1}\Delta a_1 = 0. \tag{51}$$

Combining Equations (50) and (51) we arrive at

$$\frac{\delta a_1}{\Delta a_1} = \frac{2\frac{A_0^1}{c_0^1}}{\frac{A_0^1}{c_0^1} + \frac{A_0^2}{c_0^2} + \frac{A_0^3}{c_0^3}}. \tag{52}$$

Consistent with the work on surface tidal waves [14] we define the reflection coefficient [11], R_f as the ratio of the change of pressure across the reflected wave, $\hat{\delta} p = \delta p - \Delta p$, to the change of pressure in the incident wave, Δp. From Equation (48) we note that a change in pressure is equivalent to a change in area, the reflected wave $\hat{\delta} a_1$ is defined as $\hat{\delta} a_1 = \delta a_1 - \Delta a_1$ and so the linear reflection coefficient for our problem can be written as

$$R_f = \frac{\hat{\delta} a_1}{\Delta a_1} = \frac{\frac{A_0^1}{c_0^1} - \frac{A_0^2}{c_0^2} - \frac{A_0^3}{c_0^3}}{\frac{A_0^1}{c_0^1} + \frac{A_0^2}{c_0^2} + \frac{A_0^3}{c_0^3}}. \tag{53}$$

Using the characteristic perturbation Equations (44) and (51), we further note that the linear reflection coefficient for perturbations in velocity is the negative of Equation (53), *i.e.*, $\hat{\delta} u / \Delta u = -R_f$. Finally, the transmission coefficient, T, can be defined as the ratio of the pressure perturbation transmitted to vessels 2 or 3 to the pressure perturbation in vessel 1, *i.e.*, $T = \delta p_2 / \Delta p_1 = \delta p_3 / \Delta p_1$. Since pressure is constant at the bifurcation for the linearised system, we get $T = \delta p_1 / \Delta p_1 = 1 + R_f$.

We note that the anatomical features of bifurcations in the human arterial system are such that forward-travelling waves in the parent vessel are well matched and therefore

$$\frac{A_0^1}{c_0^1} - \frac{A_0^2}{c_0^2} - \frac{A_0^3}{c_0^3} \approx 0.$$

However this necessarily means that the backwards-travelling waves are not well matched since

$$\frac{A_0^2}{c_0^2} - \frac{A_0^1}{c_0^1} - \frac{A_0^3}{c_0^3} \neq 0.$$

Two other observations on the linear reflection coefficient R_f are noteworthy. Firstly that the result for vessels 2 and 3 are analogous and can be obtained directly by permuting the vessel indices. Secondly, the symmetry between the splitting and merging junctions discussed in Section 2.2.2 implies that the reflection coefficient for the merging flows is identical to that defined by Equation (53).

2.2.4. *Terminal resistance, R_t*

The systemic and pulmonary human arterial system is a network of large arteries branching out into many smaller arteries that continue to bifurcate into arterioles and capillaries of the micro-circulation which are very small and numerous. If we are only interested in the larger arteries in the network, the problem can be reduced in size by only modelling a part of the

network. However, the networks of blood vessels further down the arterial system will also be reflecting backward-travelling waves in the body. Therefore, an approximation needs to be included for these reflections at the boundary of the modelled arteries. This introduces the concept of terminal resistance.

In the current work we adopt a definition of the terminal resistance, R_t, as the negative of the ratio of the incoming characteristic variable at the boundary, W_2, to the outgoing characteristic variable, W_1, *i.e.*,

$$R_t = -\frac{W_2}{W_1}. \tag{54}$$

In the above definition we assume that W_1 and W_2 have been defined with respect to the equilibrium state as is the case in Equations (27), (29) and (31). A value of $R_t = 1$ represents a full reflection of the outgoing wave whereas $R_t = 0$ corresponds to no reflection or an absorbing outflow. Since $u = (W_1 + W_2)/2$, the definition (54) implies that $u = W_1(1 - R_t)/2$ and so a value of $R_t = 1$ represents a total blockage condition $u = 0$.

The definition of terminal resistance given in Equation (54) has previously been adopted in the work of Wang *et al.* [11]. To relate the above definition to their work, we recall that the form of the linearised characteristic variables is given in terms of (u', p) by Equation (31) and note that the terminal resistance for this system can be defined as

$$R_t = -\frac{W_2^0}{W_1^0} = -\frac{u' - \frac{p}{\rho c_0}}{u' + \frac{p}{\rho c_0}} = -\frac{\rho c_0 - \frac{p}{u'}}{\rho c_0 + \frac{p}{u'}} = -\frac{R_p - \rho c_0}{R_p + \rho c_0}. \tag{55}$$

$R_p = p/u'$ represents the resistance of the arterial network beyond the terminal vessel. An approach for calculating the terminal resistance was proposed by Sergiopulos and Young [13] who assumed that p is the pressure upstream of the vessel and u' is the mean velocity in the terminal vessels. The mean velocity is based on the conserved distribution of blood flow in the body and the venous pressure is assumed to be zero.

3. Numerical discretisation

The principal numerical challenge of modelling the one-dimensional arterial network is to propagate waves for many periods without suffering from excessive dispersion and diffusion errors. Since the characteristic system is inherently sub-critical (*i.e.*, u $\ll c$) and does not produce shocks under physiological conditions, high-order methods are attractive due to the fast convergence of the phase and diffusion properties with the polynomial order of the scheme [22], [23, Chapters 2 and 6].

The discontinuous Galerkin formulation is a convenient formulation for high-order discretisation of hyperbolic conservation laws. Following the work of Cockburn and Shu [24] and Lomtev, Quillen and Karniadakis [25] we proceed as follows.

The one-dimensional inviscid hyperbolic system (14–15) can be written in conservative form as

$$\frac{\partial \boldsymbol{U}}{\partial t} + \frac{\partial \boldsymbol{F}}{\partial x} = 0, \quad \text{where} \quad \boldsymbol{U} = \begin{bmatrix} A \\ u \end{bmatrix}, \boldsymbol{F} = \begin{bmatrix} uA \\ \frac{u^2}{2} + \frac{p}{\rho} \end{bmatrix}. \tag{56}$$

To solve this system in a domain $\Omega = (a, b)$ discretized into a mesh of N_{el} elemental non-overlapping regions $\Omega_e = (x_e^l, x_e^u)$, such that $x_e^u = x_{e+1}^l$ for $e = 1, \ldots, N_{el}$, and

$$\bigcup_{e=1}^{N_{el}} \overline{\Omega}_e = \overline{\Omega},$$

we start by constructing the weak form (56) with respect to a set of weak vector spaces ϕ, *i.e.*,

$$\left(\frac{\partial \boldsymbol{U}}{\partial t}, \phi\right)_\Omega + \left(\frac{\partial \boldsymbol{F}}{\partial x}, \phi\right)_\Omega = 0, \tag{57}$$

where

$$(\mathbf{u}, \mathbf{v})_\Omega = \int_\Omega \mathbf{u}\,\mathbf{v}\,\mathrm{d}x.$$

is the standard $\mathbf{L}^2(\Omega)$ inner product. Decomposing the integral into elemental regions, we obtain

$$\sum_{e=1}^{N_{el}} \left[\left(\frac{\partial \boldsymbol{U}}{\partial t}, \phi\right)_{\Omega_e} + \left(\frac{\partial \boldsymbol{F}}{\partial x}, \phi\right)_{\Omega_e} \right] = 0. \tag{58}$$

Integrating the second term by parts leads to

$$\sum_{e=1}^{N_{el}} \left[\left(\frac{\partial \boldsymbol{U}}{\partial t}, \phi\right)_{\Omega_e} - \left(\boldsymbol{F}, \frac{d\phi}{dx}\right)_{\Omega_e} + [\phi \cdot \boldsymbol{F}]_{x_e^l}^{x_e^u} \right] = 0. \tag{59}$$

To get the discrete form of our problem, we choose $\boldsymbol{U}$ to be in the finite space of $\mathbf{L}^2(\Omega)$ functions which are polynomial of degree P on each element. We indicate an element of such a space using the superscript δ. We also note that $\boldsymbol{U}^\delta$ may be discontinuous across inter-element boundaries. To attain a global solution in the domain Ω we need to allow information to propagate between the elemental regions. Information is propagated between elements by upwinding the boundary flux in the third term of Equation (59). Denoting the upwinded flux as $\boldsymbol{F}^u$, we can now write the discrete weak formulation as

$$\sum_{e=1}^{N_{el}} \left[\left(\frac{\partial \boldsymbol{U}^\delta}{\partial t}, \phi^\delta\right)_{\Omega_e} - \left(\boldsymbol{F}(\boldsymbol{U}^\delta), \frac{d\phi^\delta}{dx}\right)_{\Omega_e} + \left[\phi^\delta \cdot \boldsymbol{F}^u\right]_{x_e^l}^{x_e^u} \right] = 0. \tag{60}$$

Following the traditional Galerkin approach, we choose the test function within each element to be in the same discrete space as the numerical solution $\boldsymbol{U}^\delta$. At this point, if we define our polynomial basis and choose an appropriate quadrature rule, we have a semi-discrete scheme.

Finally we select our expansion bases to be a polynomial space of order P and expand our solution on each element e in terms of Legendre polynomials $L_p(\xi)$, *i.e.*,

$$\boldsymbol{U}^\delta\big|_{\Omega_e}(x_e(\xi), t) = \sum_{p=0}^{P} L_p(\xi)\hat{\boldsymbol{U}}_e^p(t).$$

where, following standard finite-element techniques, we consider ξ in the reference element $\Omega_{st} = \{-1 \le \xi \le 1\}$ and introduce the elemental affine mapping

$$x_e(\xi) = x_e^l \frac{(1-\xi)}{2} + x_e^u \frac{(1+\xi)}{2}.$$

We note that the choice of discontinuous discrete solution and test functions allow us to decouple the problem on each element, the only link coming through the upwinded boundary fluxes. Legendre polynomials are particularly convenient because the basis is orthogonal with respect to the $\mathbf{L}^2(\Omega_e)$ inner product. To complete the discretisation, we require a time-integration scheme. In the current scheme we have adopted a second-order Adams-Bashforth scheme.

The calculation of the upwind flux $\boldsymbol{F}^u$ is an essential component of the discontinuous Galerkin formulation. Through the evaluation of the upwind flux we are able to enforce information propagation between elemental boundaries either within a single vessel or at a junction. It also allows us to impose both inflow and outflow boundary conditions in a weak sense. For an elemental boundary within a single vessel the upwinded flux is evaluated by determining the upwinded characteristic variables at the elemental interface. For the subcritical system we are considering (*i.e.*, $u < c$) this involves determining W_1 from the backward boundary and W_2 from the forward boundary. The upwinded variables (u^u, A^u) can then be determined using Equations (27) or (29) and subsequently the upwinded flux $\boldsymbol{F}^u$ is then evaluated. For bifurcations a Newton iteration is required to solve for the upwinded variables (A_1, u_1),(A_2, u_2),(A_3, u_3) as discussed in Section 2.2.1. For a more detailed discussion on the numerical implementation see reference [26].

4. Application

In this section we apply the numerical discretisation of Section 3 to the one-dimensional model network in terms of (A, u) variables as discussed in Section 2. We shall focus on two applications. In Section 4.1 we shall consider a network of 55 arteries, previously considered by Wang and Parker, and in Section 4.2 we will consider a simplified model of a reduced network to discuss the influence of a reflection at a bifurcation on the reversal of the flow waveform.

Any network of vessels can be characterised in terms of its geometrical and dynamic similarity. Geometric similarity for the one-dimensional system requires that the ratio of the vessel lengths and diameters to a characteristic scale is the same. For example, we can choose to define the network with respect to a reference diameter d_0 such as the aortic diameter. To complement the geometric similarity we also define two dynamic parameters; the Mach number, M, and the Strouhal frequency, St, defined as

$$M = \frac{u}{c_0} = u\sqrt{\rho D_0}, \qquad \mathrm{St} = \frac{d_0}{c_0 T}.$$

Recall that $c_0 = 1/\sqrt{\rho D_0}$ is the linearised wave speed and is related to the linearised distensibility D_0, ρ is the fluid density and T is the time scale of the input wave normally associated with cardiac cycle. Under the non-dimensionalisation

$$x^\star = \frac{x}{d_0}, \quad A^\star = \frac{A}{d_0^2}, \quad u^\star = \frac{u}{u_0} \quad t^\star = \frac{t}{T}, \quad p^\star = pD_0,$$

where u_0 is a characteristic convection velocity (for example the mean inflow velocity), the (A, u) system (14–15) can be written as

$$\frac{\mathrm{St}}{M_0}\frac{\partial A^\star}{\partial t^\star} + \frac{\partial A^\star u^\star}{\partial x^\star} = 0,$$

$$\frac{\mathrm{St}}{M_0}\frac{\partial u^\star}{\partial t^\star} + \frac{\partial}{\partial x^\star}\left(\frac{p^\star}{M_0^2} + \frac{(u^\star)^2}{2}\right) = 0,$$

where $M_0 = u_0/c_0$. We note that St/M_0 is essentially a Strouhal number based on u_0 rather than c_0.

4.1. Arterial network

A simplified arterial network containing the 55 largest arteries in the human body was proposed and modelled using electrical circuits by Westerhof in reference [12]. This reference provides physiological data for diameters, wall thickness, length and elastic moduli for each of the 55 arteries. Terminal resistances for the model have been calculated in [13] using the method described in Section 2.2.4. Wang and Parker [11] found that some of the bifurcations were ill-matched for forward travelling waves and the reflections that they generated obscured the reflections from the terminal segments and adjusted the diameters of the 55 arteries to give well-matched linear forward travelling waves, *i.e.*, waves that produce small reflections at the bifurcations. The bifurcations are, however, not well-matched for backward travelling waves.

We have adopted the modifications proposed in [11] to the published models [13, 12] to compute the pulsatile one-dimensional blood flow through the arterial system using the discontinuous Galerkin method. Figure 5 shows the connectivity of the arteries used in our model of the arterial network. The normalised geometry of the network and the reduced wave speed for each vessel, $c^i_{\mathrm{red}} = 1/\mathrm{St}^i = c^i_0 T/d_0$ where c^i_0 is the linearised wave speed in the i^{th} vessel, are included in Table 1.

The flow in the model arterial system is assumed initially to be at rest. A periodic half sine wave is then imposed at the ascending aorta through the forward characteristic, W_1. The values for the nonlinear and linearised model

$$W_1 = u_0 + 4c_d \qquad W_1^0 = u_0 + \frac{c_1^0}{A_0^1}a_d$$

where over each time period of length T

$$u_0 = 0, \qquad \frac{A_d(t)}{A_0^1} = \begin{cases} 1 + \sigma \sin(\pi t/0{\cdot}3) & t < 0{\cdot}3T \\ 1 & 0{\cdot}3 < t < T \end{cases}$$

$$c_d(t) = \sqrt{\frac{\beta}{2\rho}}A_d^{1/4} \qquad \text{and} \qquad a_d(t) = A_d(t) - A_0^1,$$

where $\sigma = 0{\cdot}578$ and was chosen to achieve a pressure difference of 5500 Pa over the incoming wave of a physical ascending aorta. This inflow treats the aortic valve as an absorber throughout the cardiac cycle. For all computations, second-order time integration with a time step of $\Delta t/T = 10^{-5}$ and spatial discretisation into elements of polynomial order $P = 8$ were used. In the current computations a single element was used in every vessel. A temporal and spatial convergence study has been performed in [27]. The boundary condition at the terminal vessels were imposed through a terminal resistance (see Section 2.2.4) which was either prescribed to be zero (no terminal resistance) or as given in Table 1.

To illustrate the differences in the solutions calculated using the linear and nonlinear analysis, Figure 6 shows the time histories of pressure, p, and velocity, u, at the lower end of

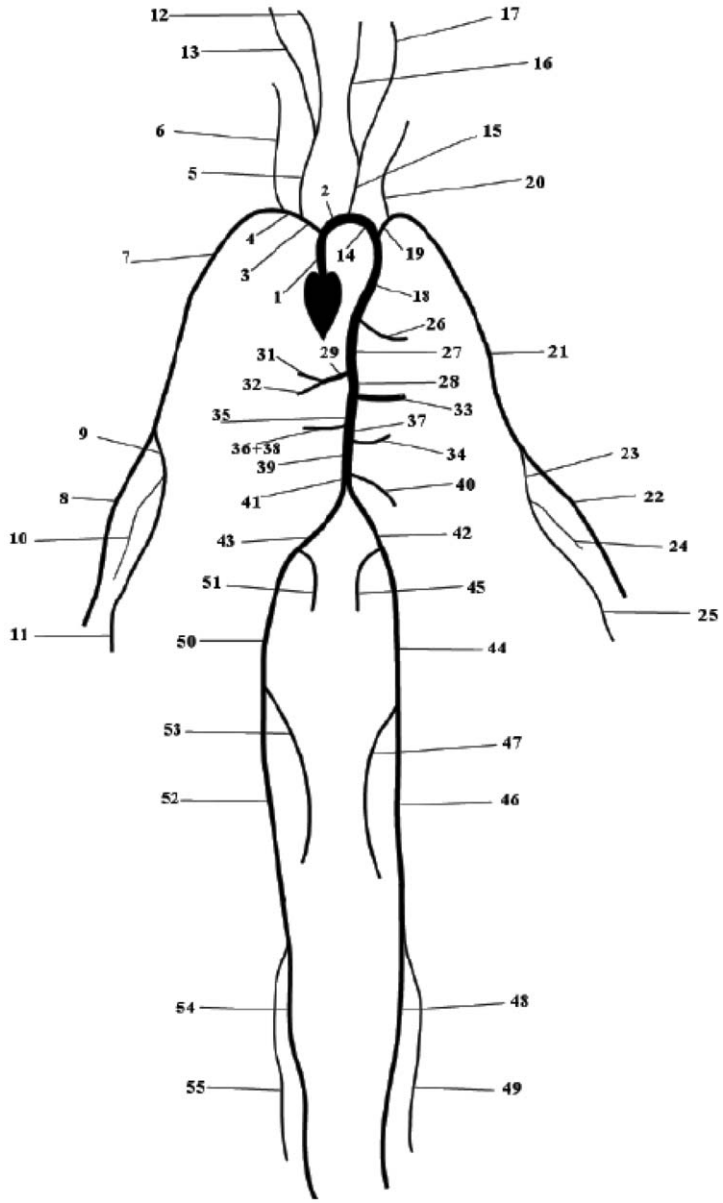

Figure 5. Connectivity of the 55 main arteries in the human arterial system.

the network (anterior tibial artery 55). No terminal resistance has been applied to the terminal vessels and the outgoing waves are therefore completely absorbed: no wave is reflected back into the system. The linear and nonlinear results are plotted on the same figure. The linear solution is represented by the solid line and the nonlinear solution is the dashed line. The bifurcations are well-matched for the linear system and there are no reflection sites within the network. Consequently the linear solution is the same shape as the input wave. We do note slight oscillations at the start of the wave $t/T = 0{\cdot}2$ which are due to numerical oscillations associated with the discontinuous nature of the derivative of the input wave in time and space. The nonlinear solution shows a small flow reversal and decrease in pressure at the tail of the

Table 1. Area A_0^i, vessel length l_i and reduced wave speed $c_0^i T/d_1$ for well-matched computational model normalised by the time period T, the aortic area $A_0^1 = \pi d_1^2/4$ and the diameter of vessel 1, d_1. This table combines the physiological data published in [13, 11, 12]. Note the absence of vessel 30 to be consistent with [11].

No.	A_0^i/A_1	l_i/d_1	c_{red}^i	R_t	No.	A_0^i/A_1	l_i/d_1	c_{red}^i	R_t
1	1·0000	1·361	158·52	–	28	0·3917	1·803	148·89	–
2	0·7382	0·680	150·36	–	29	0·1600	0·680	157·06	–
3	0·2261	1·156	161·05	–	31	0·0971	2·245	155·71	0·925
4	0·1354	1·156	167·53	–	32	0·0651	2·415	164·91	0·921
5	0·1035	6·020	173·74	–	33	0·0690	2·143	178·06	0·93
6	0·0267	5·034	291·52	0·906	34	0·1152	2·007	177·02	0·934
7	0·1227	14·354	171·71	–	35	0·3289	0·340	146·65	–
8	0·0623	7·993	230·45	0·82	36	0·0567	1·077	185·25	–
9	0·0954	2·279	214·30	–	37	0·2918	0·340	151·11	–
10	0·0174	2·687	361·71	0·956	38	0·0567	1·188	185·25	0·861
11	0·0868	5·816	219·43	0·893	39	0·2046	3·605	159·87	–
12	0·0675	5·986	231·07	0·784	40	0·0174	1·701	224·12	0·918
13	0·0675	6·020	223·23	0·79	41	0·1843	0·340	152·79	–
14	0·6608	1·327	147·68	–	42	0·1022	2·007	170·09	–
15	0·0789	7·075	185·93	–	43	0·1022	1·973	170·09	–
16	0·0516	5·986	247·12	0·784	44	0·1075	4·898	223·25	–
17	0·0516	6·020	238·74	0·791	45	0·0419	1·701	347·08	0·925
18	0·5805	1·769	149·19	–	46	0·0603	15·068	250·55	–
19	0·1040	1·156	177·64	–	47	0·0586	4·286	244·62	0·885
20	0·0191	5·034	316·98	0·906	48	0·0654	10·918	329·38	0·724
21	0·0958	14·354	182·68	–	49	0·0181	11·667	422·55	0·716
22	0·0486	7·993	245·26	0·821	50	0·1075	4·932	223·25	–
23	0·0744	2·279	228·02	–	51	0·0419	1·701	347·08	0·925
24	0·0137	2·687	384·15	0·956	52	0·0603	15·102	250·55	–
25	0·0679	5·816	233·32	0·893	53	0·0586	4·320	244·62	0·888
26	0·0465	2·721	187·16	0·627	54	0·0651	10·952	329·82	0·724
27	0·5308	3·537	145·46	–	55	0·0180	11·701	423·62	0·716

input wave when $t/T = 0{\cdot}5$. This is due to the arteries only being well matched for the linear but not for the nonlinear theory which results in a small amount of reflection and re-reflections. The nonlinear solution of p and u show that the input wave becomes skewed as the wave travels through the system. In both systems the magnitude of p remains relatively constant whilst the magnitude of u decreases.

The skewing of the nonlinear wave is due to nonlinearities introduced both in terms of the area dependent relationship of the wave speed c and the convective nonlinearity. For a forward-travelling wave the velocity and pressure variations have the same sign as shown in Figure 6. The wave speed and convective nonlinearities have a similar sign contribution which moves the nonlinear wave forward more rapidly than the linear wave. This motion causes the

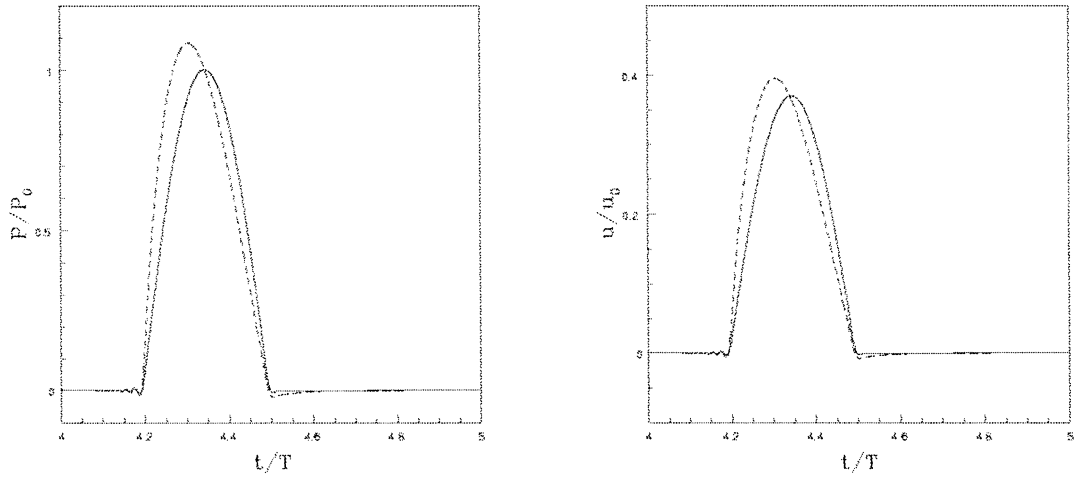

Figure 6. Linear (solid) and nonlinear (dashed) pressure and velocity histories in the anterior tibial (artery 55) of the idealised model normalised by the peak value in vessel 1. No terminal resistance is applied in this model.

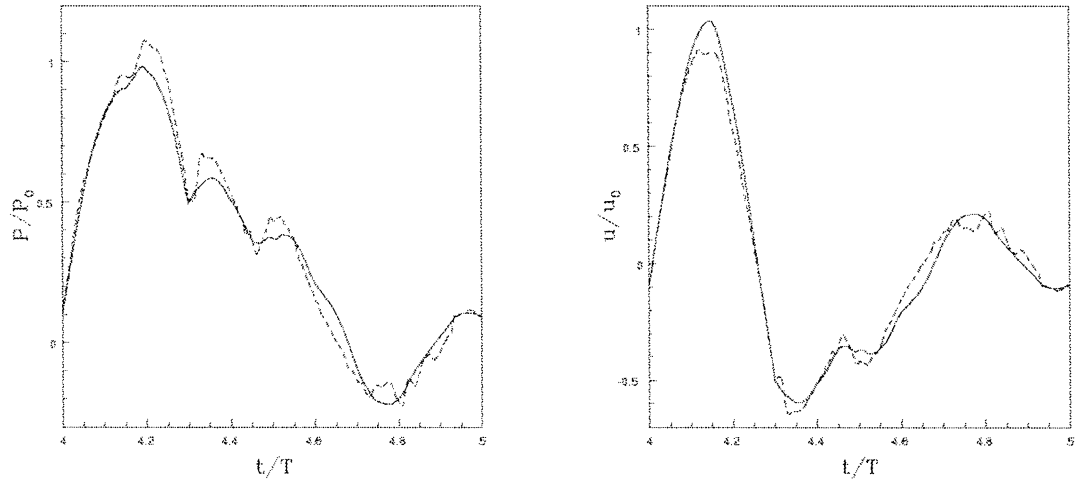

Figure 7. Linear (solid) and nonlinear (dashed) pressure and velocity histories in the ascending aorta (artery 1) of the idealised model normalised by the peak value in vessel 1. Terminal resistance is applied in this calculation according to Table 1.

pressure and velocity peak to catch up with the start of the wave. Finally we note that there is a lag of the wave in time of approximately $t/T = 0{\cdot}2$ for the input wave to reach the terminal vessels.

Figure 7 shows a comparison of the waveforms in the ascending aorta (artery 1) calculated using the linear and nonlinear models. Terminal resistances have been applied in this calculation as given in Table 1. The time u and p history plots are shown for the fifth cycle. The overall shape and magnitudes of the wave are similar for both solution methods with a slight increase in the peak pressure and a corresponding decrease in the velocity waveform. In both models the velocity peak precedes the time of the pressure peak. This is consistent with the initial contribution of the reflected waves having an additive effect to pressure and a

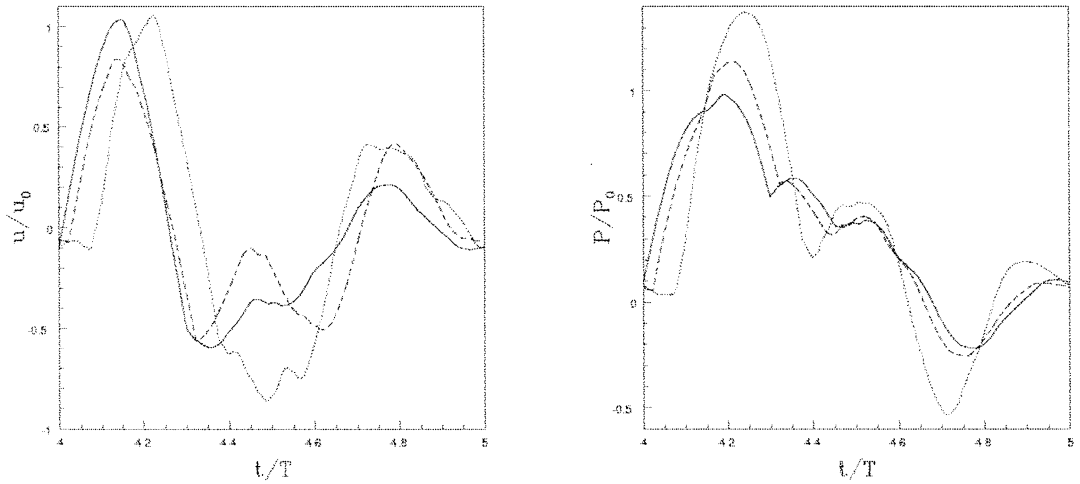

Figure 8. Linear pressure and velocity histories in; the ascending aorta (artery 1) shown by the solid line; the thoracic aorta I (artery 18) shown by the dashed line and the abdominal aorta IV (artery 39) shown by the dotted line. All values are normalised by the peak values in vessel 1. Terminal resistance is applied in this calculation according to Table 1.

subtractive effect on velocity. This property can be associated with the changes in perturbation over a backward W_2 wave, *i.e.*,

$$\Delta u + \frac{c_0}{A_0}\Delta a = 0.$$

At approximately $t/T = 4{\cdot}3$ we observe a feature similar to the dichrotic notch in the pressure waveform which is associated with the closure of the aortic valve *in vivo.* Although the action of the aortic valve is not included in this model directly the discontinuity of the imposed input velocity at $t/T = 0$ and $0{\cdot}3$ can be thought of as a function of the valve. Since we have treated the inflow as an absorber, the reflected waves are not reflected back into the system. We also note another peak in the descending part of the pressure wave which is not normally observed in the ascending aorta waveform but has been seen in waveforms further down the aorta. Uniformly increasing the wave speed of the system to $\sqrt{1{\cdot}5}c_0^i$ removes this feature.

Figure 8 shows a comparison of the pressure and velocity waveforms for arteries 1, 18 and 39 normalised by the peak values of the waveform in artery 1. From this figure we observe that the peak pressure increases as we move down the system, even though the mean pressure is observed to slowly decrease. This is in agreement with *in vivo* data [28, Chapter 8].

4.2. Flow reversal in a network

As we have seen in Section 4.1, wave reflections at arterial bifurcations and the known resistance of the system lead to different flow waveforms at different locations in the network. The shape of the flow waveform, which is measurable in the human arterial system using ultrasound techniques, is also frequently used as a diagnostic input and so it is reasonable to ask what factors influence waveform patterns such as flow reversal. To simplify the problem, we will consider a model where the peripheral resistance is low and thereby remove the contribution of wave reflections from further down the arterial tree. Physiologically, this model

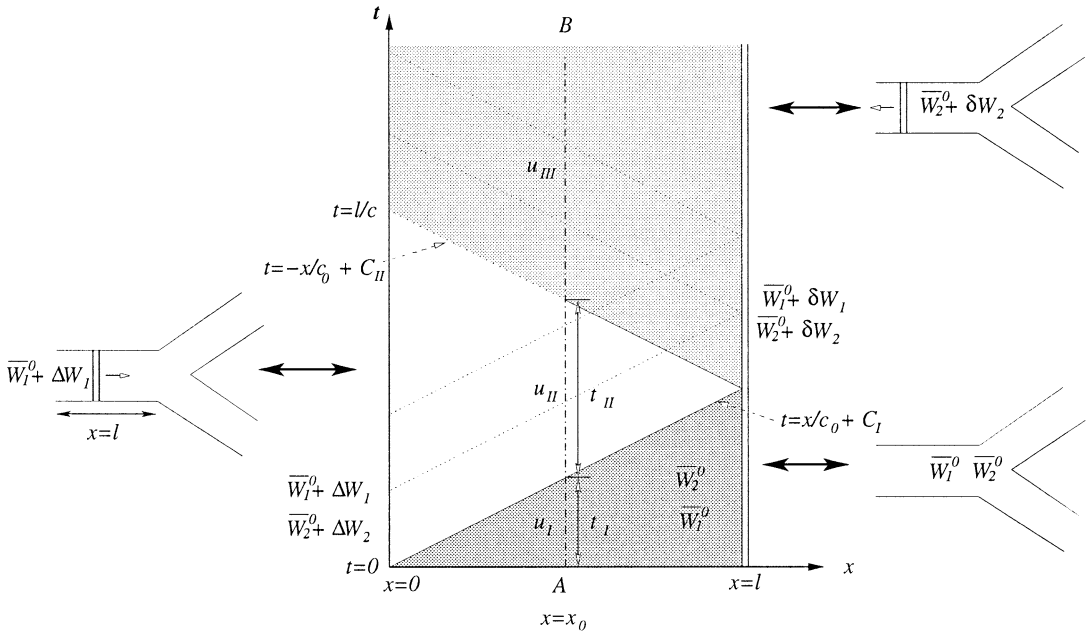

Figure 9. *x,t* plot of the parent vessel of a bifurcation expressed in terms of the characteristic variables.

might be relevant to the relatively low resistance of the vascular beds such as the cerebral system or the fetal circulation of the placenta. Therefore, examples of the model configuration might be considered appropriate to the carotid arteries or the umbilical cords. Further, as shown in MacDonald [28, Chapter 8] the flow waveform in the umbilical cord of a healthy foetus is typically positive throughout the cardiac cycle. Motivated by the observation that convective nonlinearity does not play a significant role in the wave form patterns, we will use the linearised model to analyse the system.

We consider, as shown in Figure 9, a bifurcation where the parent vessel is of length l and assume that at time $t = 0$ the solution is at a constant equilibrium state $(\bar{a}, \bar{u}')$. This state corresponds to constant equilibrium characteristic variables $\overline{W}_1^0$, $\overline{W}_2^0$ and we recall that for the linearised system

$$u' = \frac{W_1 + W_2}{2} \qquad a = \frac{A_0}{c_0}\frac{W_1^0 - W_2^0}{2}. \tag{61}$$

Introducing a perturbation to the incoming equilibrium characteristic $\overline{W}_1^0$ at the inflow to the parent vessel of the form $\Delta W_1(0, t)$ necessarily leads to a change in area and velocity, denoted as $(\Delta a, \Delta u)$, from the equilibrium values $(\bar{a}, \bar{u}')$. Since the propagation velocities λ_1^0, λ_2^0 of the characteristic variables W_1^0 and W_2^0 are $\lambda_{1,2}^0 = \pm c_0$, the characteristic variables are constant along the lines $t = \frac{x_0 \pm x}{c_0}$ in the *x,t* plot as shown in Figure 9.

To derive the velocity time history of a point x_0 as indicated by line (A-B) in Figure 9, we initially assume the boundary $x = 0$ is non-reflecting. There are then three separate solution regimes to be considered. Initially for $0 \le t < t_I$, where $t_I = \frac{x_0}{c_0}$, the solution is dictated by the equilibrium characteristics $\overline{W}_1^0$, $\overline{W}_2^0$. For the time period $t_I \le t < t_I + t_{II}$ where $t_{II} = 2\frac{l - x_0}{c_0}$ the solution is dictated by the characteristics $W_1^0 = \overline{W}_1^0 + \Delta W_1$ and $\overline{W}_2^0$. Finally for $t > t_I + t_{II}$

the solution is dependent on the incoming forward characteristic $W_1^0 = \overline{W}_1^0 + \Delta W_1$ and the reflected backward characteristic, $W_2^0 = \overline{W}_2^0 + \delta W_2$ where δW_2 is the reflected state after ΔW_1 reaches the bifurcation at $x = l$. Denoting the velocity at $x = x_0$ in the three temporal regimes as $u_I(t)$, $u_{II}(t)$ and $u_{III}(t)$, we note from Equation (61) that

$$u(x_0, t) = \begin{cases} u_I(t) &= \frac{\overline{W}_1^0 + \overline{W}_2^0}{2} & t < t_I \\ u_{II}(t) &= \frac{\overline{W}_1^0 + \Delta W_1 + \overline{W}_2^0}{2} & t_I < t < t_I + t_{II} \\ u_{III}(t) &= \frac{\overline{W}_1^0 + \Delta W_1 + \overline{W}_2^0 + \delta W_2}{2} & t_I + t_{II} < t \end{cases}, \tag{62}$$

where $t_I = \frac{x_0}{c_0}$, $t_{II} = 2\frac{l - x_0}{c_0}$.

Since the velocity $u_I(t)$ is only determined by the equilibrium values $\overline{W}_1^0$ and $\overline{W}_2^0$, we can immediately state that

$$u_I(t) = \frac{\overline{W}_1^0 + \overline{W}_2^0}{2} = \bar{u}'.$$

To obtain an expression for $u_{II}(t)$ we need to relate the perturbation $\Delta W_1(0, t)$ to a change in velocity $\Delta u(0, t)$. In general a change in the inflow conditions can lead to a change in $\Delta W_1(0, t)$ and $W_2^0(0, t)$ such that

$$\begin{aligned} W_1^0(0, t) &= \overline{W}_1^0 + \Delta W_1(0, t), \\ W_2^0(0, t) &= \overline{W}_2^0 + \Delta W_2(0, t), \end{aligned}$$

where

$$\overline{W}_{1,2}^0 = \bar{u}' \pm \frac{c_0}{A_0}\bar{a}, \tag{63}$$

$$\Delta W_{1,2} = \Delta u \pm \frac{c_0}{A_0}\Delta a. \tag{64}$$

For $t < \frac{2l}{c_0}$ the reflected wave has not reached the inflow boundary at $x = 0$. Therefore $W_2^0(0, t)$ must remain constant and

$$\Delta W_2 = 0 \quad \Rightarrow \quad \Delta u(0, t) = \frac{c_0}{A_0}\Delta a(0, t) \qquad 0 \le t < \tfrac{2l}{c_0}. \tag{65}$$

Keeping the inflow as an absorbing boundary for $t > \frac{2l}{c_0}$ requires that $\Delta W_2(0, t) = \delta W_2(0, t - \frac{l}{c_0})$.

Using condition (65) in Equation (64), we can relate $\Delta W_1(0, t)$ to $\Delta u(0, t)$ through

$$\Delta W_1(0, t) = 2\Delta u(0, t) \qquad 0 \le t < \tfrac{2l}{c_0}. \tag{66}$$

Noting that $\Delta W_1(x_0, t) = \Delta W_1(0, t - t_I)$, we obtain

$$u_{II}(t) = \frac{\overline{W}_1^0 + \Delta W_1^0(0, t - t_I) + \overline{W}_2^0}{2} = \bar{u}' + \Delta u(0, t - t_I)$$

for $t < t_I + t_{II}$.

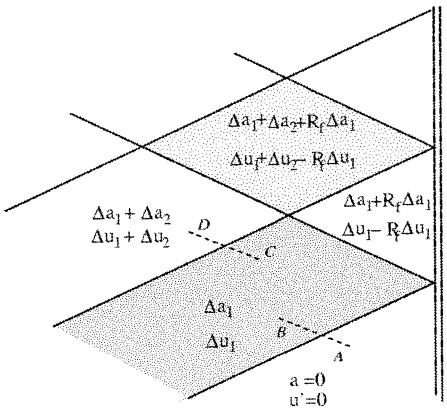

Figure 10. Decomposition of incoming wave at the bifurcation into incremental components.

At $t = l/c_0$ the perturbed incoming characteristic $W_1^0 + \Delta W_1$ reaches the bifurcation at $x = l$ and after a linear reflection we have a new characteristic state

$$W_{1,2}^0(l,t) = \overline{W}_{1,2}^0 + \delta W_{1,2}(l,t), \qquad \text{where} \qquad \delta W_{1,2} = \delta u(l,t) \pm \frac{c_0}{A_0}\delta a(l,t).$$

From Section 2.2.3 we recall that for a linear reflection

$$\frac{\hat{\delta} a}{\Delta a} = -\frac{\hat{\delta} u}{\Delta u} = R_f,$$

where

$$\delta a = \Delta a + \hat{\delta} a \quad \text{and} \quad \delta u = \Delta u + \hat{\delta} u$$

and

$$\begin{aligned} \delta W_2(l,t) &= \Delta u(l,t) - \frac{c_0}{A_0}\Delta a(l,t) - Rf\left[\Delta u(l,t) + \frac{c_0}{A_0}\Delta a(l,t)\right] \\ &= \Delta W_2(l,t) - R_f \Delta W_1(l,t). \end{aligned} \tag{67}$$

We have previously seen that $\Delta W_2(0,t) = 0$ for $t < t_I$. It is, however, not immediately evident that this condition at $x = 0$ can be applied at $x = l$, since the two boundaries are connected by a W_1 forward characteristic. Nevertheless, we recall that the backward characteristic W_2 relates information across the W_1 characteristic and this observation leads to the condition $\Delta W_2(l,t) = 0$. To illustrate this result, we consider the example shown in Figure 10 where we decompose an incoming wave into incremental piecewise constant components, *i.e.*,

$$\Delta u(t) = \begin{cases} \Delta u_1 & t < \Delta\tau_1 \\ \Delta u_1 + \Delta u_2 & \Delta\tau_1 \le t \le \Delta\tau_2 \\ \vdots & \vdots \end{cases}.$$

If we consider the backward characteristic labelled *A*-*B* in Figure 10, the state Δa_1, Δu_1 is related to the equilibrium state $\bar{a} = 0, \bar{u}' = 0$ along the backward characteristic through the expression

$$\Delta u_1 - \frac{c_0}{A_0}\Delta a_1 = 0. \tag{68}$$

Similarly along the characteristic line marked *C-D* in Figure 10 we have that

$$\Delta u_1 + \Delta u_2 - \frac{c_0}{A_0}(\Delta a_1 + \Delta a_2) = \Delta u_1 - \frac{c_0}{A_0}\Delta a_1$$

which implies that

$$\Delta u_2 - \frac{c_0}{A_0}\Delta a_2 = 0. \tag{69}$$

An analogous argument indicates that conditions (68) and (69) also hold after the reflection. From this we deduce that $\Delta W_2(l, t) = 0$ for all time, and equation (67) becomes

$$\delta W_2(l, t) = -R_f \Delta W_1(l, t). \tag{70}$$

Finally since $u_{III}(t)$ is determined by the forward characteristic $\overline{W}_1^0 + \Delta W_1(0, t)$ and backward characteristic, $\overline{W}_2^0 + \delta W_2(l, t)$ then, applying Equations (70), we obtain

$$u_{III}(t) = \bar{u}' + \Delta u(0, t - t_I) - R_f \Delta u(0, t - t_{II}), \tag{71}$$

where

$$\delta W_2(x_0, t) = \delta W_2(l, t - \tfrac{l - x_0}{c_0}) = -R_f W_1(0, t - t_{II})$$

and we have assumed that $\Delta W_1(0, t)$ obeys relation (66) for all time. The evaluation of $u(0, t)$ from Equation (62) only equals $\Delta u(0, t)$ for $t < \frac{2l}{c_0}$ since the reflection wave will reach the absorbing inflow boundary after this time.

In summary, for an incoming wave defined by $\Delta W_1(0, t) = 2\Delta u(0, t)$, the velocity history at point $x = x_0$ is

$$u(x_0, t) = \begin{cases} \bar{u}' & t < t_I \\ \bar{u}' + \Delta u(0, t - t_I) & t_I < t < t_I + t_{II} \\ \bar{u}' + \Delta u(0, t - t_I) & \\ \qquad -R_f \Delta u(0, t - t_I - t_{II}) & t_I + t_{II} < t \end{cases}. \tag{72}$$

If $x = 0$ is taken to be a non-reflecting boundary, we should expect an infinite series of reflected waves from the junctions at both ends of the vessel. The initial solution will be identical to Equation (72) up to the time $t < 3t_I + t_{II}$ after which time the incoming wave has reflected from both the ends of the vessel and return to point $x = x_0$. Realising that an analogous reflection occurs as a backward W_2 characteristic meets the left boundary (*i.e.*, $\delta W_1 = -R_f^l \Delta W_2$), we can define the velocity time history at $x = x_0$ in a vessel between two bifurcations as

$$\begin{aligned} u(x_0, t) \;=\; & \Delta u(0, t - t_I) - R_f^r \Delta u(0, t - t_I - t_{II}) \\ + \quad & \sum_{n=1}^{\infty} (R_f^l)^n (R_f^r)^n \; \Delta u(0, t - (2n+1)t_I - n\, t_{II}) \\ - \quad & \sum_{n=1}^{\infty} (R_f^l)^n (R_f^r)^{n+1} \; \Delta u(0, t - (2n+1)t_I - (n+1)t_{II}), \end{aligned} \tag{73}$$

where R_f^l and R_f^r are the reflections from the left and right boundaries, respectively, and $\Delta u(0, \tau) = 0$ for $\tau < 0$.

4.2.1. *Results*

An initial observation from Equations (72) and (73) is that, if R_f^l, $R_f^r < 0$, then $(R_f^l)^n(R_f^r)^n$ and $-(R_f^l)^n(R_f^r)^{n+1}$ are both positive. Therefore, provided that $\Delta u(0,t)$ and $\bar{u}'$ are both positive, the velocity history at any point in the vessel will remain positive. In stating this result we have also assumed that there are no significant reflected waves from other vessels which is true when the terminal resistance is small. The condition $R_f < 0$ requires that

$$\frac{A_0^1}{c_0^1} < \frac{A_0^2}{c_0^3} + \frac{A_0^2}{c_0^3},$$

where the superscripts refer to the parent ('1'), and daughter vessels ('2' and '3') as introduced in Section 2.2.3.

As previously mentioned, a physiological example of vessels perfusing a bed of relatively low terminal resistance are the umbilical arteries where, for a healthy foetus, the flow waveform is strictly positive. From anatomical measurement of placenta casts, we have calculated reflection coefficient at the downstream end of two umbilical arteries of $R_f^r = -0{\cdot}5$ and $R_f^r = -0{\cdot}4$ (based upon area measurements and assuming constant wave speed). In a normal arterial bifurcation the upstream reflection coefficient is typically also negative since, physiologically, forward-travelling waves are well matched. Assuming this at the upstream bifurcation to the umbilical arteries leads to the prediction of a positive flow waveform by the above analysis. Under abnormal conditions where the terminal resistance is increased, the possibility of negative waves entering from a terminal reflection is introduced. This is consistent with the medical practise of using a flow reversal as a diagnostic indicator.

When $R_f > 0$, the velocity contribution from the reflected wave at the bifurcation is negative and so some period of reversed flow can exist in our simplified model. This is illustrated in Figure 11 where we show a single bifurcation model. In this model we consider three vessels where each vessel is $20D$ long where D is the diameter of the parent vessel. The reduced wave speed $c_{\text{red}} = Tc_0/D$ of a vessel with a diameter of $D = 2{\cdot}5$cm, a time period $T = 1$ sec and a wave speed of $c_0 = 3$ m/s is $c_{\text{red}} = 120$. To match these conditions in our example we keep $T = 1$ and set the model wave speed to be $c_0^{\text{model}} = 120$ in all vessels. Considering a peak physiological inflow to be 25 cm/s implies that the Mach number is $M = u/c_0 = 1/12$. Matching this Mach number in our model therefore requires a peak input velocity of $u = Mc_0^{\text{model}} = 10$. Finally, to generate a linear reflection of $R_f^l = 0{\cdot}5$, we specify that the daughter vessels have a diameter of $D/\sqrt{6}$. The input for this problem was prescribed to be

$$\Delta W_1(0,t) = 2\Delta u(0,t) = 20\sin^2(3\pi t)H(t-1/3), \tag{74}$$

where $H(\tau)$ is the Heaviside step function. The inflow boundary imposes a positive sinusoidal velocity inflow over a third of the characteristic period and all backwards waves are completely absorbed. All computations were performed with a single element representing each vessel and an 11th order polynomial expansion within each element. A second-order time-stepping scheme was applied with a non-dimensional time step of $\Delta t/T = 0{\cdot}001$.

Figure 11 shows the time history of the velocity and area normalised by the peak velocity and equilibrium area in the parent vessel. Also indicated by the dashed line in Figure 11(c) is the analytic solution due to the single reflection at the bifurcation. As can be seen in this figure and previously shown by Equation (72), the solution is simply comprised of the incoming wave and a time-shifted reflected wave. The positive reflection coefficient means that the sign

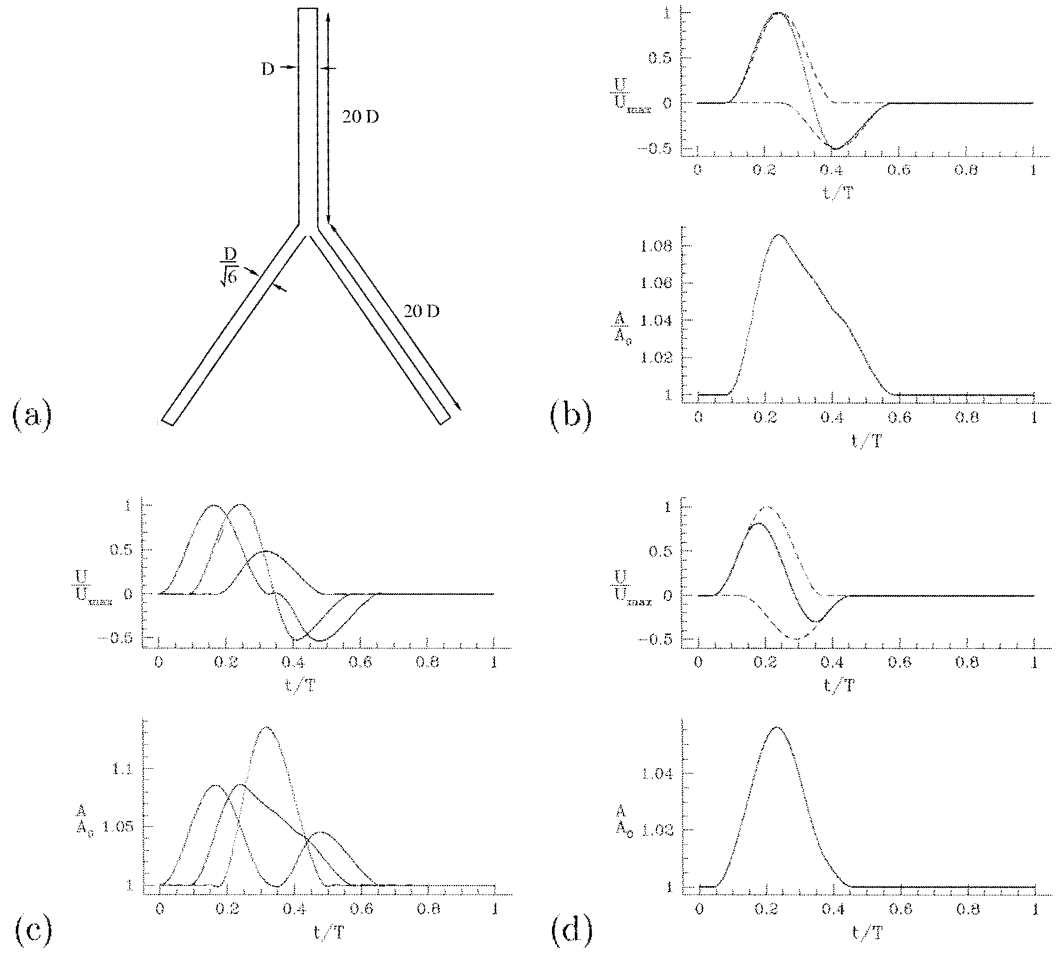

Figure 11. Linearised reflection from a single bifurcation. a) Model configuration. b) velocity and area history at the centre of the parent vessel. c) velocity and area time history at the beginning, middle and end of the parent vessel. d) velocity and area time history at the centre of the parent vessel when wave speed is doubled.

of the velocity perturbation due to the reflected wave is the opposite of the incoming velocity. Due to the phase shift the summation of the two waves causes a flow reversal the temporal extent of which is of the order $O(t_{II})$ where we recall that $t_{II} = 2(l - x_0)/c_0$.

This point is further highlighted in Figure 11(c) where we show the time history at the beginning (inflow), middle and end (bifurcation) of the parent vessel. The first wave form corresponds to the history point at the inflow of the vessel. Since at this point $x_0 = 0$ and t_{II} is maximal, there is a significant phase shift between the incoming and reflected waves. The dimensions of the problem are such that at $x_0 = 0$ $t_{II} = 2 \times 20/120 = 1/3$ which is exactly the time period of the input pulse and so we observe two distinct waves. Considering the history point at the bifurcation, *i.e.*, $x_0 = 20D$, we observe an opposite effect: there is no phase shift and the velocity profiles therefore cancel leading to a single velocity peak of magnitude $u/u_{\max} = 0{\cdot}5$. This interaction also has an additive effect on the area variation causing a maximal deflection.

Figure 11(d) shows the same example considered in Figure 11(b) but where the wave speed has been doubled and all numerical parameters are kept fixed. This has the effect of halving

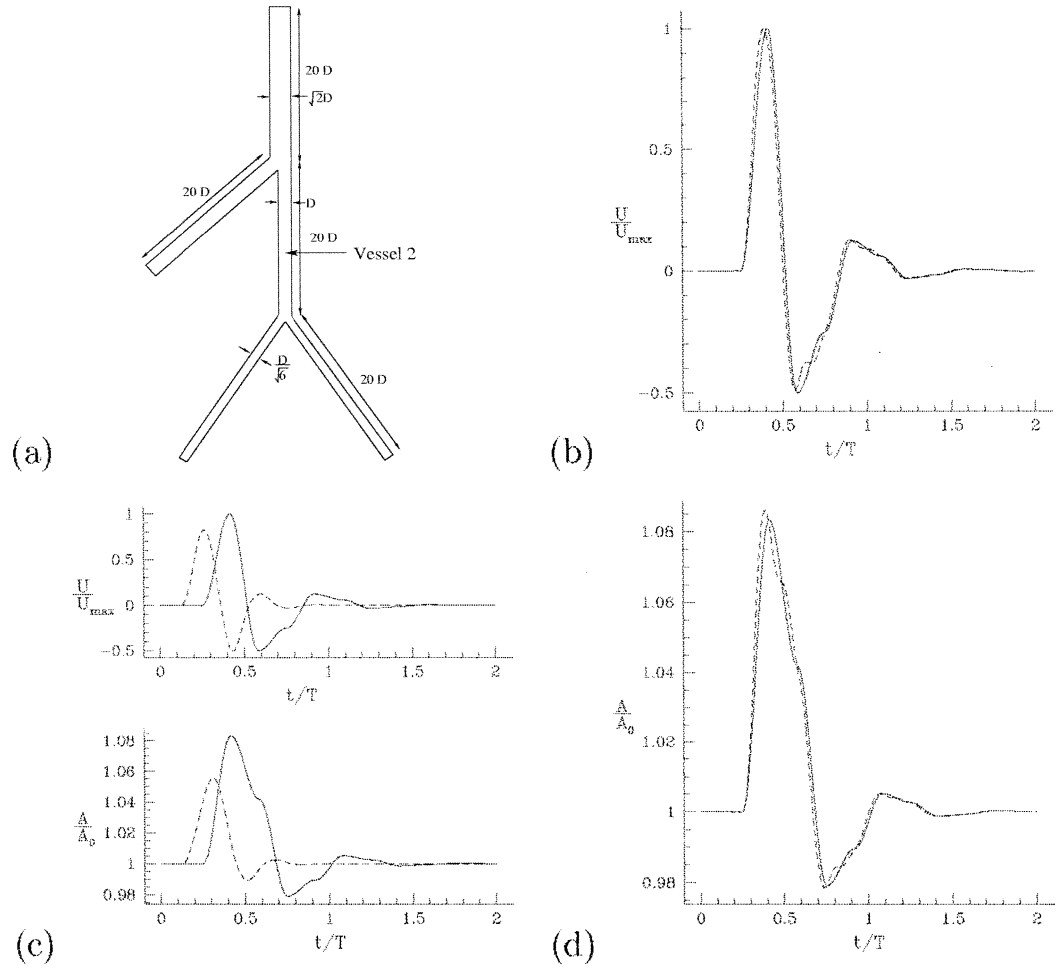

Figure 12. Linearised reflection of a vessel between two bifurcations ($R^l_f = -0{\cdot}5$, $R^r_f = 0{\cdot}5$) a) Model configuration. b) Comparison of linear (solid) and nonlinear (dashed) velocity history. c) Velocity and area time history in the middle of vessel 2 using a wave speed of c_0 (solid) and $2c_0$ (dashed). d) Comparison of linear (solid) and nonlinear (dashed) area time history. All time histories are evaluated at the centre of vessel 2.

both t_I (the time for the wave to reach x_0) and t_{II} although the inflow wave pulse still has a non-zero contribution for a time of $T/3$. As indicated by the dashed lines there is a more significant overlap between the incoming and reflected wave. This larger overlap leads to a reduction in the velocity peak and the extent of the flow reversal regime. A reduction in flow reversal has been observed *in vivo* in [29] where an increase in wave speed was induced through an association of smoking with arterial stiffness.

To complete our wave form analysis we consider a two bifurcation model as shown in Figure 12 (a) and applying the same numerical resolution as the previous example. In this problem the bottom three vessels are identical to the previous case shown in Figure 11. The two additional upstream vessels are configured so that the upstream bifurcation of vessel 2 has a reflection coefficient of $R^l_f = -0{\cdot}5$. This can be achieved by using the same wave speed c_0 in all vessels, making the daughter vessels of the same diameter and setting the parent vessel diameter to $\sqrt{2}D$. Figures 12(b) and (d) show the velocity history evaluated at the centre

of vessel 2 over two time periods using the input wave (74). The solid line represents the linear model which is indistinguishable from the solution given by Equation (73) evaluated with $n = 50$ terms. Also indicated in this plot is the nonlinear solution shown as a dashed line. As observed previously, the nonlinear solution is not significantly different from the linear solution. The most significant differences are due to the different phase properties of the nonlinear solution. Finally in Figure 12(c) we compare the linear model using a wave speed of c_0, as indicated by the solid lines, compared to a wave speed of $2c_0$ as indicated by the dashed lines. Once again we observe the greater wave cancellation for the case with a higher wave speed and the faster decay associated with faster wave reflections.

5. Discussion and concluding remarks

Three-dimensional simulation of haemodynamics in anatomically accurate geometries has gained a great deal of attention over the last decade. Despite this growing interest, numerical simulation of reduced modelling, such as the one-dimensional vascular system discussed in this paper, still offer equally important insight into the physiological behaviour of the haemodynamics in the human vascular system. Indeed, the large range of scales within the human circulation imply that a combination of these techniques will be required for accurate, patient specific modelling, as advocated in [19]. Nevertheless the long length scales of pulse waves in the human systemic system compared to the characteristic diameter of many vessels suggest that the strength of the coupling of the three-dimensional haemodynamics to the one-dimensional model will be relatively small, thereby supporting the concept of independently studying the reduced model.

The advent of new imaging modalities, such as Magnetic Resonance Imaging, and the availability of computational methods developed for compressible flows now offer the potential to solve efficiently the 1-D models in anatomically correct, patient specific arterial systems [30, 31, 27]. Furthermore the relatively inexpensive cost of these numerical methods for large networks (*i.e.*, of the order of minutes in a network of 55 arteries [27]) as compared to cost of three-dimensional modelling makes the reduced method potentially attractive for a clinical environment if the model is appropriately validated. Accordingly there is a need to understand the mathematical and physical motivation behind the derivation of the models, particularly in the time-domain, rather than the frequency domain, where most of the numerical methods are normally applied.

In this paper we have detailed the formulation of the linear and nonlinear systems. We have also outlined the formulation of different choices of solution variables as well as the widely applied, zero-dimensional, Windkessel model [16]. Starting from the conservative system in terms of (A, u) variables, we then reviewed the nonlinear characteristic system which is often necessary for many hyperbolic numerical methods. The characteristic system, combined with mass and total-pressure conservation at a junction, then provided a consistent way to extend the single vessel model to a bifurcating network. Within the context of the method of characteristics for the linear system, we have also presented a characteristic, time-domain derivation of the classical results for the reflection and transmission coefficients of waves at bifurcations. In the human systemic system, unlike the pulmonary system, the high characteristic wavespeed as compared to the average sectional velocity means that this linearised analysis can be applied with some confidence to interpret the wave reflections in the system. [11, 10, 26, 27].

Using a spectral/hp element spatial discretisation with a discontinuous Galerkin Formulation, we have supported the formulation of the model system by solving a network of 55 arteries originally studied by Wang and Parker [10, 11]. In previous work [26], we have presented results in different vessels of this model network. In this paper we have focused on demonstrating the limited role of nonlinearities in the model by numerically comparing the solution to the linear and nonlinear models within the network. As has been previously reported [10], the role of nonlinearity is relatively small (of the order of 10%) thereby justifying the use of linearised analysis for this case. We remark, however, that the computational effort in solving the nonlinear equations with an explicit method is not significantly different from solving the linear equations. However, the nonlinear equations also permits more general properties, such as taper and variable wall characteristics, to be implicitly included.

Under physiological conditions, the weak role of nonlinearity in the systemic system also motivated the application of the linearised analysis to understand the conditions required at a bifurcation to produce a non-reversing flow waveform. Using the methods of characteristics and linearised reflection coefficients, we have presented a derivation of the time history of the flow waveform in a bifurcating network of three vessels with low terminal resistance. This analysis demonstrated that the linearised reflection coefficient needs to be negative to maintain non-reversing flow in the parent vessel which can be achieved if the ratio of the area to the wave speed is smaller in the parent vessel than the summation of this ratio in the two daughter vessels. The analysis was also supported by numerical examples.

Although many components of the results and formulations presented in this paper are available in past literature, we believe it is valuable to assemble the information in a single presentation. A complete derivation of the linear and nonlinear governing equations is important not only for the application of many numerical methods, which typically require time-domain formulations, but also in interpreting the results produced from these numerical models. We would also advocate that the time-domain analysis provides a physically intuitive way to interpret the model which is not always immediately available when treating the linear equations in the frequency domain. Currently this type of analysis is being applied to more complex models of monochorionic placenta networks [31] as well as the arterial network of a single human subject [27].

Acknowledgements

The authors would like to acknowledge Professor Luca Formaggia of the Politecnico di Milano and Dr Ling Wee of the Queen Charlotte's hospital for their contributions. Partial support of the work is acknowledged under EU grant HPRN-CT-2002-00270.

References

1. L. Euler, Principia pro motu sanguinis per arterias determinando. *Opera posthuma mathematica et physica anno 1844 detecta*, 2 (1775) 814–823. ediderunt PH Fuss et N Fuss Petropoli; Apund Eggers et Socios.
2. T. Young, Hydraulic investigations, subservient to an intended Croonian lecture on the motion of the blood. *Phil. Trans. R. Soc. London* 98 (1808) 164–186.
3. A.I. Moens, Over de voortplantingssnelheid von den pols (On the speed of propagation of the pulse). Technical report, Leiden (1877).
4. D.J. Korteweg, Über die Fortpflanzungsgeschwindigkeit des Schalles in elastischen Röhren. *Ann. Phys. Chem. (NS)* 5 (1878) 525–527.

5. B. Riemann, Gesammelte mathematische Werke und wissenschaftlicher Nachlass. Leipzig, B.G. Teubner (ed.), (1876) 145–164 (originally published as Über die Fortpflanzung ebener Luftwellen von endlicher Schwingungsweite. Technical report, Göttingen 8 (1860) 43.
6. J.C. Stettler, P. Niederer and M. Anliker, Theoretical analysis of arterial hemodynamics including the influence of bifurcations. part i: Mathematical model and prediction of normal pulse patterns. *Ann. Biomed. Engng.* 9 (1981) 145–164.
7. J.C. Stettler, P. Niederer and M. Anliker, Theoretical analysis of arterial hemodynamics including the influence of bifurcations, part ii: Critical evaluation of theoretical model and comparison with noninvasive measurements of flow patterns in normal and pathological cases. *Ann. Biomed. Eng.* 9 (1981) 165–175.
8. R. Skalak, The synthesis of a complete circulation, In: D. Bergel (ed.), *Cardiovascular Fluid Dynamics* (vol. 2). London: Academic Press (1972) pp. 341–376.
9. J.R. Womersley, An elastic tube theory of pulse transmission and oscillatory flow in mammalian arteries. Technical Report WADC Technical Report TR 56-614, Wright Air Development Center (1957).
10. J.J. Wang, *Wave Propagation in a Model of the Human Arterial System.* PhD thesis, Imperial College, University of London, U.K. (1997) 181 pp.
11. J.J. Wang and K.H. Parker, Wave propagation in a model of the arterial circulation. To appear in *J. Biomech.* (2004).
12. N. Westerhof and A. Noordergraaf, Arterial viscoelasticity: a generalized model. effect on input impedence and wave travel in the systemic tree. *J. Biomech.* 3 (1970) 357–379.
13. N. Stergiopulos, D.F. Young and T.R. Rogge, Computer simulation of arterial flow with applications to arterial and aortic stenoses. *J. Biomech.* 25 (1992) 1477–1488.
14. Sir Horace Lamb, *Hydrodynamics*. New York: Dover, (1945) 738 pp.
15. M.J. Lighthill, *Waves in Fluids.* Cambridge: Cambridge University Press (1978) 504 pp.
16. O. Frank, Die Grundform des arteriellen Pulses. *Z. Biol.* 37 (1899) 483–526.
17. O. Frank, Die Theorie der Pulswellen, *Z. Biol.* 85 (1926) 91–130.
18. J.J. Wang, A.B. O'Brien, N.G. Shrive, K.H. Parker and J.V. Tyberg, Time-domain representation of ventricular-arterial coupling as a windkessel and wave system. *Am. J. Physiol-Heart C* 284 (2003) H1358–H1368.
19. L. Formaggia, J.-F. Gerbeau, F. Nobile and A. Quarteroni, On the coupling of 3D and 1D Navier-Stokes equations for flow problems in compliant vessels. *Comp. Meth. in Appl. Mech. Engng.* 191 (2001) 561–582.
20. S. Canic and E.H. Kim, Mathematical analysis of the quasilinear effects in a hyperbolic model of blood flow through compliant axi-symmetric vessels. *Math. Methods Appl. Sci.* 26 (2003) 1–26.
21. L. Formaggia, F. Nobile and A. Quarteroni, A one dimensional model for blood flow: application to vascular prosthesis. In: I. Babuška, T. Miyoshi, and P.G. Ciarlet, (ed.) *Mathematical Modeling and Numerical Simulation in Continuum Mechanics*; volume 19 of Lecture Notes in Computational Science and Engineering. Berlin: Springer-Verlag (2002) pp. 137–153.
22. S.J. Sherwin, Dispersion analysis of the continuous and discontinuous Galerkin formulations. In: B. Cockburn, G.E. Karniadakis and C.W. Shu, (ed.) *Discontinuous Galerkin methods: Theory, Computational and Applications.* Berlin: Springer (2000) pp. 425–431.
23. G. Em Karniadakis and S.J. Sherwin, *Spectral/hp Element Methods for CFD.* New York: Oxford University Press (1999) 390 pp.
24. B. Cockburn and C.W. Shu. TVB Runge-Kutta projection discontinuous Galerkin finite element methods for conservation laws II general framework. *Math. Comm.* 52 (1989) 411–435.
25. I. Lomtev, C.B. Quillen and G.E. Karniadakis, Spectral/hp methods for viscous compressible flows on unstructured 2d meshes. *J. Comp. Phys.* 144 (1998) 325–357.
26. S.J. Sherwin, L. Formaggia, J. Peiró and V. Franke, Computational modelling of 1D blood flow with variable mechanical properties and its application to the simulation of wave propagation in the human arterial system. Accepted by *Int. J. Num. Meth. Fluids* (2003).
27. Victoria Franke, *One Dimensional Spectral/hp Element Simulation of Wave Propagation in Human Arterial Networks.* PhD thesis, Imperial College London (2003) submitted.
28. W.W. Nichols and M.F. O'Rourke, *McDonald's Blood Flow in Arteries: Theoretical, Experimental and Clinical Principles*, 4th edition London: Arnold (1998) 564 pp.
29. C.G. Caro, M.J. Lever, K.H. Parker and P.J. Fish, Effect of cigarette smoking on the pattern of arterial blood flow: possible insight into mechanisms underlying the development of arteriosclerosis. *The Lancet* (1987) 11–13.

30. N.P. Smith, A.J. Pullan and P.J. Hunter, An anatomically based model of transient coronary blood flow in the heart. *SIAM J. Appl. Math.* 62 (2002) 990–1018.
31. V. Franke, S.Sherwin, K. Parker, N. Watkins, W. Ling and N.M. Fisk, Time domain computational modelling of 1D arterial networks in the Placenta. *ESAIM: Mathematical Modelling and Numerical Analysis.* To appear (2003).